iScience

CellPress
OPEN ACCESS

Article

Intranasal vaccination with a Newcastle disease virus-vectored vaccine protects hamsters from SARS-CoV-2 infection and disease

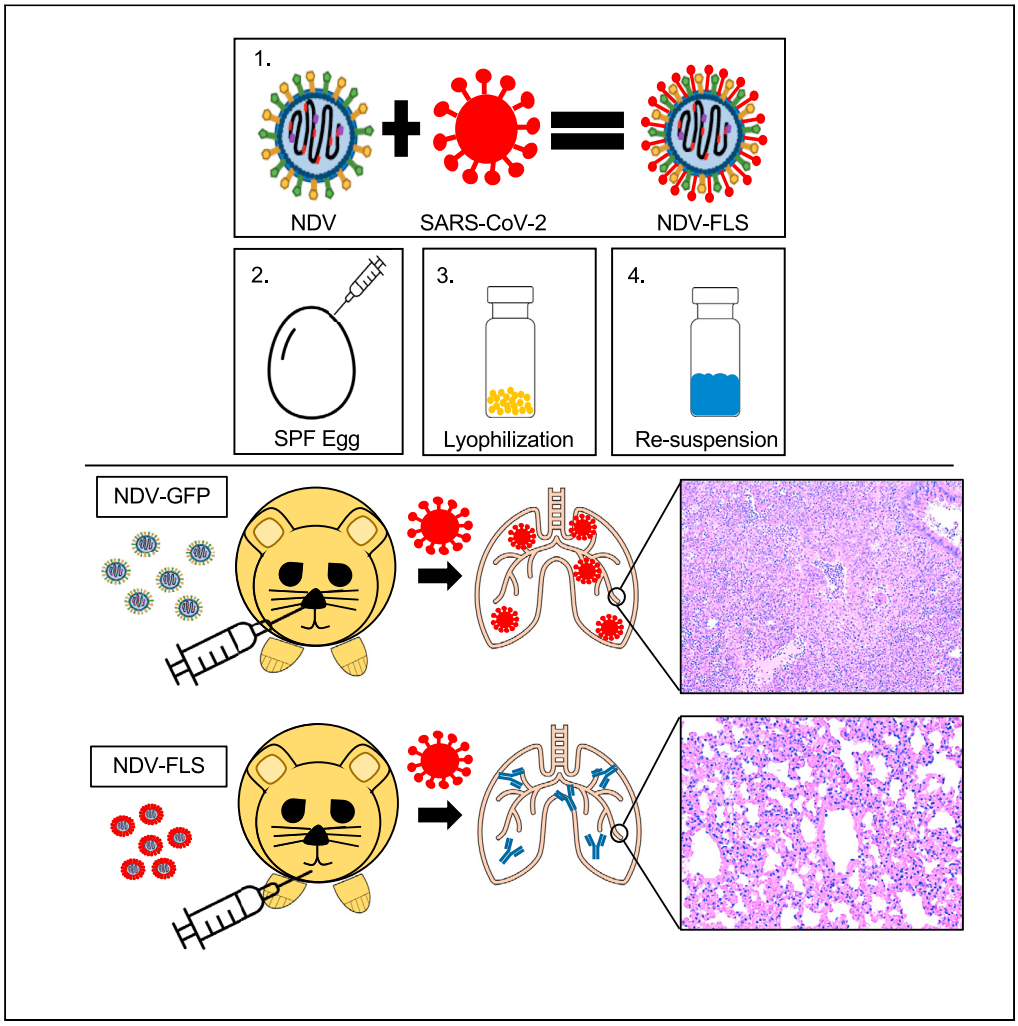

Bryce M. Warner, Lisa A. Santry, Alexander Leacy, ..., Leonardo Susta, Darwyn Kobasa, Sarah K. Wootton

kwootton@uoguelph.ca

Highlights

Recombinant NDV passively incorporates SARS-CoV-2 spike into the virion

Vaccination with NDV expressing SARS-CoV-2 spike protects hamsters from disease

No infectious SARS-CoV-2 was detectable in the lungs of vaccinated hamsters

NDV-vectored vaccines represent a viable option for protection against COVID-19

Warner et al., iScience *24*, 103219
November 19, 2021
https://doi.org/10.1016/j.isci.2021.103219

iScience

CellPress
OPEN ACCESS

Article

Intranasal vaccination with a Newcastle disease virus-vectored vaccine protects hamsters from SARS-CoV-2 infection and disease

Bryce M. Warner,[1,5] Lisa A. Santry,[2,5] Alexander Leacy,[2,5] Mable Chan,[1,5] Phuc H. Pham,[2,5] Robert Vendramelli,[1,5] Yanlong Pei,[2,5] Nikesh Tailor,[1,5] Emelissa Valcourt,[1] Anders Leung,[1] Shihua He,[1] Bryan D. Griffin,[1] Jonathan Audet,[1] Marnie Willman,[3] Kevin Tierney,[1] Alixandra Albietz,[1] Kathy L. Frost,[1] Jacob G.E. Yates,[2] Robert C. Mould,[2] Lily Chan,[2] Yeganeh Mehrani,[2] Jason P. Knapp,[2] Jessica A. Minott,[2] Logan Banadyga,[1] David Safronetz,[1,3] Heidi Wood,[1] Stephanie Booth,[1] Pierre P. Major,[4] Byram W. Bridle,[2,6] Leonardo Susta,[2,6] Darwyn Kobasa,[1,3,6] and Sarah K. Wootton[2,6,7,*]

SUMMARY

The pandemic severe acute respiratory syndrome coronavirus 2 (SARS-CoV-2) is the cause of coronavirus disease 2019 (COVID-19). Worldwide efforts are being made to develop vaccines to mitigate this pandemic. We engineered two recombinant Newcastle disease virus (NDV) vectors expressing either the full-length SARS-CoV-2 spike protein (NDV-FLS) or a version with a 19 amino acid deletion at the carboxy terminus (NDV-Δ19S). Hamsters receiving two doses (prime-boost) of NDV-FLS developed a robust SARS-CoV-2-neutralizing antibody response, with elimination of infectious virus in the lungs and minimal lung pathology at five days post-challenge. Single-dose vaccination with NDV-FLS significantly reduced SARS-CoV-2 replication in the lungs but only mildly decreased lung inflammation. NDV-Δ19S-treated hamsters had a moderate decrease in SARS-CoV-2 titers in lungs and presented with severe microscopic lesions, suggesting that truncation of the spike protein was a less effective strategy. In summary, NDV-vectored vaccines represent a viable option for protection against COVID-19.

INTRODUCTION

The novel severe acute respiratory syndrome coronavirus-2 (SARS-CoV-2) emerged in late 2019 in the city of Wuhan, mainland China, as the causative agent of a severe respiratory disease named *coronavirus disease 2019* (COVID-19) (Andersen et al., 2020; Zhou et al., 2020). The virus has been classified in the *Coronaviridae* family, β-coronavirus genus, and *Sarbecovirus* subgenus (i.e., β-coronavirus subgroup B) (Lu et al., 2020). Phylogenetic analysis has shown that this virus shares ~50% genetic similarity with Middle East respiratory syndrome-CoV, ~80% similarity with SARS-CoV, and >90% similarity with bat β-coronaviruses, suggesting spillover of the virus from bats to humans, possibly through an intermediate adaptive host (El Zowalaty and Jarhult, 2020; Frutos et al., 2020; Lu et al., 2020).

On March 11, 2020, a COVID-19 global pandemic was declared by the World Health Organization (WHO), and by April 2021, the disease had spread worldwide, with over 146 million confirmed cases and more than three million deaths ((WHO), last accessed 2020.09.07). Crude fatality rates have been reported to be around 4% (Karadag, 2020; Verity et al., 2020), although recent estimates that adjusted for demography and case under-ascertainment range between 0.15 and 1.5% (Ioannidis, 2021; Mallapaty, 2020; Russell et al., 2020). The elderly, people with hypertension, immunosuppression, diabetes, and obesity, among other pre-existing conditions, are at a heightened risk of developing severe disease (Williamson et al., 2020).

SARS-CoV-2 is transmitted through respiratory droplets and contact routes (Chan et al., 2020b; Li et al., 2020a; Liu et al., 2020; Ong et al., 2020). In people with severe disease, morbidity and mortality are

[1]Zoonotic Diseases and Special Pathogens, Public Health Agency of Canada, Winnipeg, Canada

[2]Department of Pathobiology, University of Guelph, Guelph, Canada

[3]Department of Medical Microbiology and Infectious Diseases, University of Manitoba, Winnipeg, Canada

[4]Juravinski Cancer Centre, 699 Concession Street, Hamilton, ON L8V 5C2, Canada

[5]These authors contributed equally

[6]Senior authors

[7]Lead contact

*Correspondence: kwootton@uoguelph.ca

https://doi.org/10.1016/j.isci.2021.103219

mediated by severe respiratory distress syndrome and vascular disease. The former is caused by diffuse alveolar damage associated with virus replication in type I and II alveolar pneumocytes (Bradley et al., 2020; Calabrese et al., 2020; Martines et al., 2020). Lesions not associated with the respiratory system include endothelial damage, thrombosis, and disseminated intravascular coagulation; however, compelling evidence of virus replication in the endothelium is lacking both in human natural cases or animal models (Besutti et al., 2020; Bradley et al., 2020; Martines et al., 2020; Sia et al., 2020; Varga et al., 2020). Molecular effectors of tissue damage include unchecked production of pro-inflammatory cytokines (i.e., cytokine storm), decreased angiotensin-converting enzyme-2 (ACE2) activity, and activation of a thrombo-inflammatory cascade leading to a hypercoagulable state (Domingo et al., 2020).

Not surprising, multiple research groups have developed vaccine platforms against SARS-CoV-2, including recombinant viral vectors, nucleic acids (DNA, mRNA, and self-replicating RNA), protein subunits, virus-like particles, and live-attenuated or inactivated SARS-CoV-2 virions (Jeyanathan et al., 2020). The vast majority of these vaccines target the SARS-CoV-2 spike (S) protein, the main target antigen for neutralizing antibodies against the virus (Ziegler et al., 2020). By the spring of 2021, in the United States and Canada, two mRNA vaccines, as well as one or two adenovirus-vectored vaccines, respectively, have been approved for emergency use (https://www.who.int/publications/m/item/draft-landscape-of-covid-19-candidate-vaccines). However, it is unclear how these vaccines will be able to curtail the spread of and morbidity caused by novel SARS-CoV-2 variants, such as the B.1.351 (South African variant) and B1.617.2 (Indian/Delta variant), which have been detected since late 2020 (Kirola, 2021) (Kupferschmidt, 2021). Evolution of variants of concerns has highlighted the importance of sterilizing immunity to prevent circulation of SARS-CoV-2 in a partially vaccinated population, an occurrence that can promote development of escape virus mutants due to immunological selective pressure (Peiris and Leung, 2020).

Newcastle disease virus (NDV) has been extensively investigated as a candidate recombinant live vaccine platform for human and veterinary infectious diseases (Kim and Samal, 2016) and shows great potential as a vaccine against SARS-CoV-2 (Shirvani and Samal, 2020). NDV is the type-species of the avian orthoavulavirus-1 (AOaV-1) group, in the *Paramyxoviridae* family (Rima et al., 2019); this virus is enveloped and has a non-segmented, negative-strand RNA genome that allows insertion of foreign genes (up to ~5kb), which are stably expressed at high levels (Zhao et al., 2015). The use of NDV as a candidate vaccine vector in humans offers several advantages. As an avian virus, NDV is antigenically distinct from common human vaccines and pathogens, avoiding the problem of pre-existing immunity that would limit its efficacy in people (Capua and Alexander, 2004). More importantly, as an oncolytic agent NDV has shown an excellent safety profile, whereby direct intravenous, aerosol, or intratumoral administration of large doses of the virus are well tolerated in people (Csatary et al., 1993; Pecora et al., 2002; Wheelock and Dingle, 1964). As a vaccine vector in pre-clinical models, NDV has been shown to be safe and protective in non-human primate models of infection with pathogenic avian influenza virus, Ebola virus, and SARS-CoV (Bukreyev et al., 2005; DiNapoli et al., 2007, 2010). Lastly, NDV is an acute cytoplasmic virus with an encapsidated genome, mitigating concerns about recombination or tissue persistence (Afonso, 2008; Shirvani and Samal, 2020).

In this study, we show the efficacy of an intra-nasally delivered, non-virulent NDV vaccine expressing the SARS-CoV-2 S protein in a Syrian hamster model of COVID-19, by analysis of nasal and lung tissues at the peak of SARS-CoV-2 replication. The use of a non-virulent NDV strain (*i.e.*, lentogenic pathotype which does not cause disease in poultry) circumvents regulatory restriction associated with livestock safety (Cattoli et al., 2011), and the intranasal delivery was aimed at developing mucosal, as well as systemic immunity (Calzas and Chevalier, 2019).

RESULTS

Development of recombinant NDV vectors expressing SARS-CoV-2 spike proteins

In this study, we utilized a fully synthetic molecular clone of lentogenic NDV (LaSota strain, GenBank: AF077761.1) flanked at the 5′ end by a T7 promoter followed by three non-templated G's and at the 3′ by a self-cleaving hepatitis delta virus ribozyme and a T7 terminator sequence (Figure 1A). The ribozyme, by self-cleaving immediately at the end of the viral antigenomic transcript, ensures adherence to the "rule of six" of genomic length (Kolakofsky et al., 1998). The synthetic genome was designed to contain an additional transcriptional cassette between the phosphoprotein (P) and the matrix (M) genes, which was flanked by unique XbaI and MluI restriction sites (to facilitate transgene insertion), and gene start and gene end signals (to promote transcription by the viral polymerase) (Park et al., 2006). An additional L289A mutation

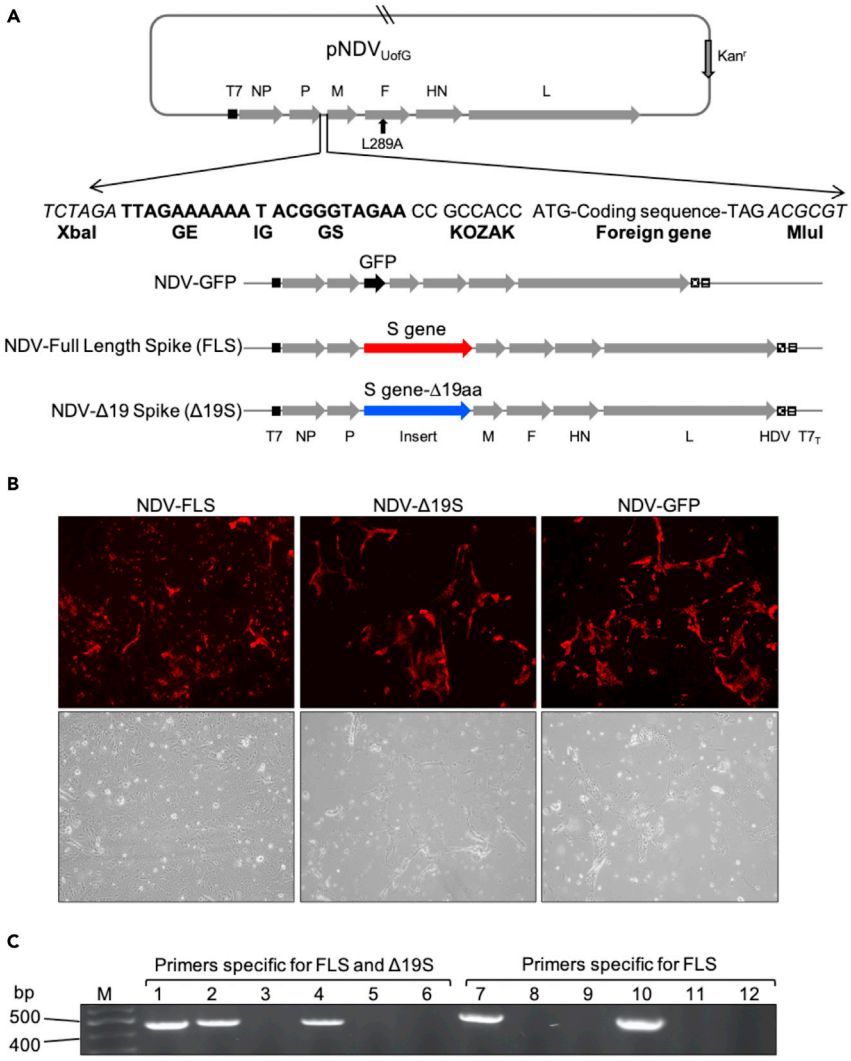

Figure 1. Generation of recombinant NDV vectors expressing the Spike (S) gene from SARS-CoV-2

(A) Schematic representation showing the recombinant NDV genome with XbaI and MluI restriction sites introduced between the P and M genes, where the GFP, full-length spike (FLS) and C-terminal truncated spike (Δ19S) genes were inserted.

(B) Virus replication and cytopathic effect in cells. DF-1 cells were infected with NDV-FLS, NDV-Δ19S, and NDV-GFP virus at a multiplicity of infection (MOI) of 10. The first row shows immunofluorescence (red fluorescence) for NDV nucleoprotein; the second row shows bright field. Both NDV-FLS and NDV-Δ19S replicated in cells, showing expression of NDV nucleoprotein, and caused cytopathic effect similar to the NDV-GFP control.

(C) Agarose gel electrophoresis of PCR-amplified products from DF-1 cells infected with recombinant NDV engineered to express the SARS-CoV-2 S protein. DF-1 cells were infected with either NDV-FLS, NDV-Δ19S, or NDV-GFP. RNA was extracted from cells 12 h later and reverse transcribed to cDNA. Primers were used to target both the FLS and the Δ19S (lanes 1–6); or only the full-length spike (lanes 7–12). (1, 7) NDV-FLS; (2, 8) NDV-Δ19S; (3, 9) NDV-GFP; (4, 10) infectious clone of NDV-full-length spike (positive control); (5, 11) uninfected DF1 (negative control); (6, 12) no-template control. M = GeneRuler 50 bp DNA Ladder (Thermo Fisher Scientific).

in the fusion (F) gene was included to enhance fusogenicity (Sergel et al., 2000). Three recombinant NDV vectors were designed by cloning in a transcriptional cassette expressing either (1) the complete coding sequence of human codon-optimized SARS CoV-2 S protein (NDV-FLS), (2) the partial coding sequence of human codon-optimized spike protein possessing a 19 amino acid deletion from the C-terminus (NDV-Δ19S), and (3) the coding sequence of the enhanced green fluorescent protein (GFP), an immunologically irrelevant protein, to be used as a control (NDV-GFP) (Figure 1A). The truncated version of the spike protein was included as this mutation has been shown to promote more efficient incorporation of spike into

lentiviral particles and vesicular stomatitis virus (Fukushi et al., 2005; Johnson et al., 2020) particles. Successful rescue of recombinant viruses was verified by immunofluorescence staining for the ribonucleoprotein (RNP) complex in NDV-FLS-, NDV-Δ19S-, and NDV-GFP-infected DF-1 chicken fibroblasts (Figure 1B), and by reverse transcription polymerase chain reaction (RT-PCR) to confirm insertion of the spike gene in the viral genome (Figure 1C).

The full-length, but not the Δ19 truncated version, of SARS-CoV-2 spike protein is efficiently incorporated into NDV virions

Western blot analysis of whole cell lysates from DF-1 cells infected at the same multiplicity of infection (MOI = 1) with NDV-FLS or NDV-Δ19S showed robust expression of the full-length S protein at approximately 180 KDa, which was more intensely expressed in NDV-Δ19S- compared with NDV-FLS-infected cells (Figure 2A). Similarly, the cleaved S2 subunit migrated at approximately 100 KDa and was more intensely expressed in NDV-Δ19S- compared with NDV-FLS-infected cells (Figure 2A). To investigate whether the S protein expressed by the NDV vector would be incorporated into the virion and to compare expression with the challenge virus, SARS-CoV-2 and vaccine viruses (NDV-FLS and NDV-Δ19S) were subjected to Western blot analysis. As shown in Figure 2B, SARS-CoV-2 virions incorporated approximately equal amounts of uncleaved and cleaved S protein, as shown by bands right below 200 KDa and one at 100 KDa, respectively, while the virion of the NDV-FLS virus incorporated almost exclusively cleaved S protein. Despite the fact that NDV-Δ19S- infected cells expressed more S protein, this was poorly incorporated into the NDV-Δ19S virions. Nevertheless, S protein expressed from NDV migrated with a similar molecular weight and pattern to that of SARS-CoV-2 S protein.

When incorporated in the NDV virion, the S protein appeared in the cleaved form at around 100 KDa. This suggests efficient cleavage due to the multibasic cleavage site (Ou et al., 2020), a feature that was likely enhanced by the proteolytic activity of the allantoic fluid (Kandeil et al., 2014), as NDV-FLS and NDV-Δ19S were grown in eggs.

Taken together, these data demonstrate that NDV can be engineered to express the SARS-CoV-2 spike protein and that the full-length spike protein is incorporated into the NDV virion more efficiently than the Δ19 truncated version.

NDV vectors expressing SARS-CoV-2 spike proteins do not show an altered infectivity

To test whether the spike protein incorporation into the NDV virion would increase NDV infectivity, we conducted virus neutralization assays in HEK 293T cells over-expressing human ACE2, the receptor for SARS-CoV-2 (Ziegler et al., 2020). Mouse serum, which successfully neutralized lentiviral particles pseudotyped with the S protein in a separate experiment, did not neutralize NDV-FLS or NDV-Δ19S as shown by immunofluorescent staining for NDV RNP at three days post-infection (Figure S2). Instead, immune serum from chickens vaccinated with NDV completely neutralized the viruses (Figure S2). This indicates that incorporation of S protein on the surface of the NDV virion does not alter infectivity or tropism of the vaccine backbone.

To investigate whether expression of the S protein would impact the fusogenic properties of the recombinant NDV vaccines, DF-1 cells were infected with NDV-FLS, NDV-Δ19S, or NDV-GFP, and the number of nuclei was averaged over the total number of cells, with syncytia counted as one cell. As shown in Figure 2C, all three viruses formed syncytia in the presence of trypsin; however, NDV-FLS showed a significantly decreased fusogenic activity compared with either NDV-Δ19S or NDV-GFP (Figure 2D).

Finally, to confirm that the modifications to the NDV vector did not alter its virulence in poultry, we determined the mean death time (MDT) of NDV-FLS, NDV-Δ19S, and NDV-GFP in embryonated chicken eggs. All viruses had an MDT >110 h and thus retained their lentogenic phenotype. Overall, these data demonstrate that NDV engineered to express the SARS-CoV-2 spike protein do not display an altered safety profile *in vitro* and *in ovo*.

NDV vectors expressing SARS-CoV-2 spike proteins are immunogenic in hamsters

We wanted to determine whether vaccination with either the NDV expressing full-length or the truncated spike protein would protect against disease in a hamster model of SARS-CoV-2 infection. Groups of ten Syrian hamsters received intranasal instillations of 10^7 plaque-forming units (PFUs) of either NDV-FLS,

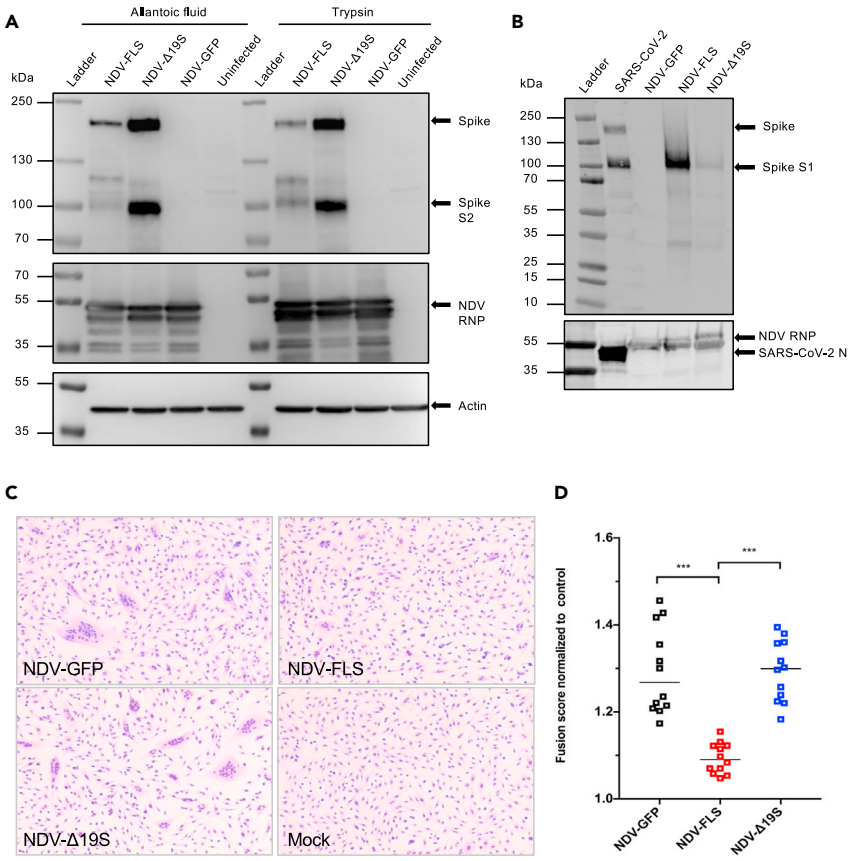

Figure 2. Expression of the spike (S) protein by recombinant NDV vaccines

(A) Western blot analysis of whole cell lysates from DF-1 cells infected with recombinant NDV viruses to confirm S protein expression. Cells were infected with an MOI of 1 with either NDV-FLS, NDV-Δ19S, NDV-GFP, or media only (control), in the presence of allantoic fluid (left) or trypsin (right) for proteolytic activity. Immunoblotting was done 24 h post infection, using rabbit-anti-S2 subunit, mouse-anti-NDV ribonucleoprotein (RNP), and mouse-anti-actin. Full and cleaved S protein (180 KDa and 100 KDa, respectively) are found at much larger amounts in the lysate from NDV-SΔ19-infected cells compared with those infected with NDV-FLS. No S protein expression is observed in cells infected with NDV-GFP or uninfected cells (control). Infection was confirmed by presence of bands corresponding to the RNP of NDV in infected cells.

(B) To compare the incorporation, cleavage, and migration patterns of the S protein between the challenge virus and the vaccine candidates, we conducted Western blot analysis of purified SARS-CoV-2, NDV-FLS, NDV-Δ19S, and NDV-GFP. Equal amounts of purified virus (1.0×10^7 plaque-forming units [PFUs]) were resolved on an SDS-PAGE gel and used for Western blot employing the following primary antibodies: a rabbit anti-S1 (top blot), a rabbit anti-SARS-CoV-2 nucleocapsid, and a mouse anti-NDV RNP (bottom blot). The blot shows incorporation of approximately equal amounts of both full-length and cleaved S protein into the SARS-CoV-2 virion, with bands migrating slightly below 220 KDa and at 100 KDa, respectively. NDV-FLS virions show prominent incorporation of cleaved S protein, while NDV-Δ19S shows significantly less incorporation of cleaved S protein. The NDV-GFP control shows no transgene expression.

(C) For the fusogenicity assay, DF-1 cells were grown in 6-well plates and infected with NDV viruses at an MOI of 0.1. Cells were maintained in Dulbecco's Modified Eagle Medium (DMEM) with 2% FBS supplemented with 5% allantoic fluid. 24 hpi media was removed, cells were washed in PBS, fixed with methanol/acetone for 20 min at −20°C, and stained with crystal violet. (D) The fusogenicity score was calculated dividing the number of nuclei by the number of cells in four fields of view per each of the three biological replicates. Counting was assisted using ImageJ (U.S. National Institutes of Health, Bethesda, Maryland, USA). The score for each virus was normalized to the non-infected negative control. Shown are data medians with data scatterplot (n = 3/group). Statistical significance was assessed by using the Kruskal-Wallis and Dunn's test for multiple comparisons. *** = <0.001

NDV-Δ19S, or NDV-GFP (control), as part of a single dose or a two-dose schedule (Figure 3A). At 29 days after the first vaccine dose, low anti-SARS-CoV-2 immunoglobulin (IgG) titers were detected by enzyme-linked immunosorbent assay (ELISA) in the serum of hamsters receiving the NDV-FLS vaccine, while the

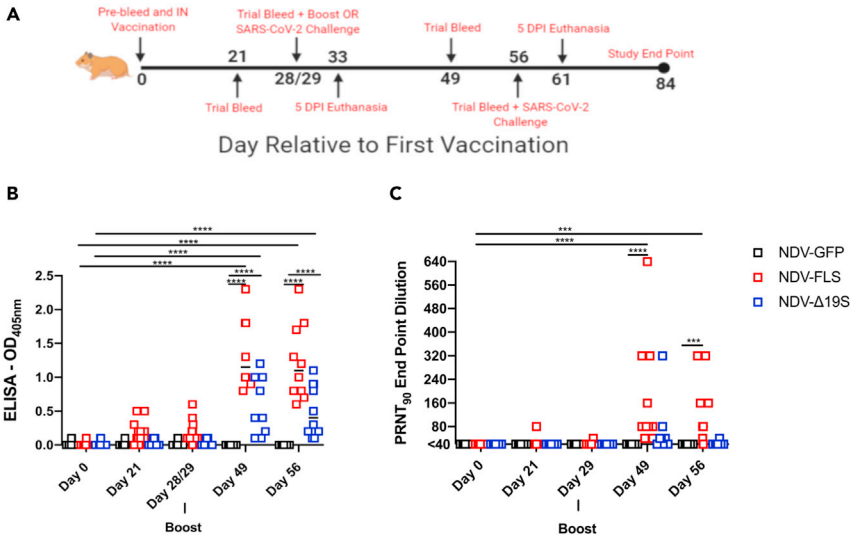

Figure 3. Antibody responses in NDV vaccinated hamsters

Groups of 10 hamsters were vaccinated via intranasal route with 10^7 PFU of NDV expressing either GFP (NDV-GFP), full-length SARS-CoV-2 spike (S) protein (NDV-FLS), or truncated SARS-CoV-2 S protein (NDV-Δ19S), either in a single-dose or a homologous prime-boost schedule 28 days apart. Hamsters were challenged 28 days after prime or boost (A). The concentration of S protein-specific IgG in the serum (diluted 1:400) of vaccinated hamsters was assessed by enzyme-linked immunosorbent assay (ELISA), and is reported as optical density (OD) (B). The levels of neutralizing antibodies in the serum were assessed by plaque reduction neutralization assay 90% ($PRNT_{90}$) (C). Shown are data scatterplots with medians (n = 10/group). Statistical significance was assessed by two-way ANOVA with multiple comparisons. *** = <0.001, **** = <0.0001.

IgG levels in the NDV-Δ19S-treated animals were indistinguishable from those treated with NDV-GFP (Figure 3B). Neutralizing antibodies, detected by plaque reduction neutralization test ($PRNT_{90}$) titers, were only detectable in a single animal in the NDV-FLS group prior to the second vaccine dose (Figure 3C). Following a second homologous vaccine dose, a substantial induction of anti-SARS-CoV-2 humoral immune responses occurred, with a significant increase in serum IgG titers seen in both vaccine groups (Figure 3B), and a significant increase in $PRNT_{90}$ titers in hamsters receiving NDV-FLS (Figure 3C). Only two (of ten) NDV-Δ19S-vaccinated hamsters had $PRNT_{90}$ titers detectable 20 days following the second dose; however, this response waned by the challenge day (Figure 3C). The serum concentration of anti-SARS-CoV-2 IgG and neutralizing titers were significantly higher in the NDV-FLS-treated group, compared to the NDV-Δ19S- and NDV-GFP-treated groups, suggesting that incorporation of the spike protein into the NDV virion may be required for stronger induction of antibody responses. Our data show that a homologous prime-boost vaccination with NDV expressing SARS-CoV-2 spike protein is highly immunogenic in hamsters.

Vaccination of hamsters with NDV vectors expressing SARS-CoV-2 S protects against SARS-CoV-2-induced clinical signs and pathology

To determine whether immune responses in animals receiving a single dose or a homologous prime-boost would result in protection from disease, each of the groups of hamsters described above, which were vaccinated with 10^7 PFU NDV-FLS, NDV-Δ19S, or NDV-GFP, were challenged with 10^5 fifty-percent tissue culture infective dose ($TCID_{50}$) of SARS-CoV-2 on day 56 post-vaccination. An additional experiment was carried out by infecting hamsters at 28 days after receiving the prime only, using the same methodology. Animals were weighed and monitored daily for signs of disease throughout the course of infection. Of ten animals in each group, four were kept for 28 days to examine any differences in weight loss and long-term outcome of infection, while six were euthanized on day five post-infection to examine pathology and viral loads in the tissues during acute infection.

In the single-dose group, NDV-FLS-vaccinated hamsters had significantly less weight loss on day 4 post-infection compared with the NDV-GFP and NDV-Δ19S-vaccinated hamsters. The NDV-Δ19S-vaccinated hamsters showed similar weight loss to controls, including several animals that lost greater than 10% of their initial weight within five days (Figure 4A). In the prime-boost group, the mean weight loss of the

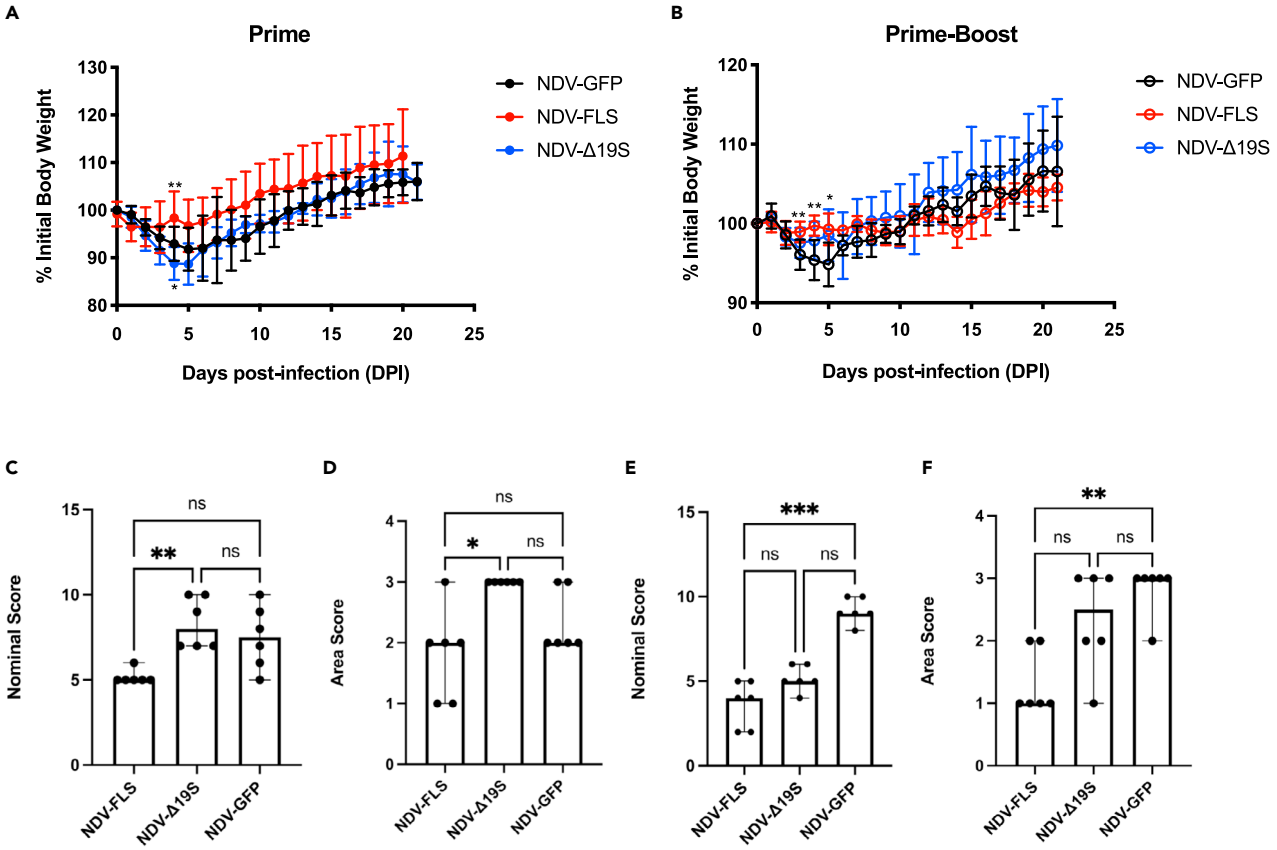

Figure 4. Protective efficacy of NDV vaccines against SARS-CoV-2 infection

Vaccinated hamsters were challenged via intranasal inoculation with 10^5 mean tissue culture infectious dose ($TCID_{50}$) of SARS-CoV-2. Weights of hamsters in the prime (A) or prime-boost (B) schedule were evaluated through day 28 post-challenge (n = 10 or 4/group). At day 5 post-challenge, 6 hamsters per group (n = 6/group) were euthanized and the severity of microscopic lesions for the prime only (C and D) and prime-boost groups (E and F) were assessed. Lesions were evaluated by tallying presence of nominal disease pathology categories (C and E), or by assessing the percentage of affected lung on section (D and F). For graphs A-B, a two-way ANOVA mixed effects model with Tukey's multiple comparison test was run to compare differences in weight between each group at each time point. Circles indicate means. Error bars indicate SD. For graphs C–F, columns represent median +/− range; statistical significance was assessed by Kruskal-Wallis and Dunn's test for multiple comparisons. * = <0.05, ** = <0.01, *** = <0.001.

NDV-FLS-treated hamsters was significantly less than NDV-GFP-treated hamsters on days 3, 4, and 5 post-infection (Figure 4B). Surprisingly, in the NDV-GFP-vaccinated animals, we did not see the weight loss that is typically seen in our hamster model and that has been reported by other groups (Imai et al., 2020). Of the four animals that were not euthanized, none reached greater than 5% weight loss following infection throughout the 28 days, while five of six of the euthanized animals had as high as 8% weight loss and were trending downward. These animals were likely euthanized before reaching peak weight loss, thereby artificially skewing the mean weight loss of that group.

The magnitude of microscopic lesions in the lungs was assessed semi-quantitatively, in order to evaluate the efficacy of the vaccine candidates to decrease the severity of lesions associated with SARS-CoV-2 infection. For both the prime and prime-boost experiments, nominal reporting of lesion categories for each hamster is summarized in Tables S1 and S2, while the extent of affected lung tissue area is reported in Table S3.

Lesions in the control hamsters were similar between the prime only and prime-boost groups (Table S2; see below for a detailed description of histopathology). In the prime only cohort,when the compound score of nominal categories was considered, NDV-FLS-treated hamsters had significantly lower scores compared to the NDV-Δ19S-, but not the NDV-GFP-treated group (Figure 4C). Similarly, NDV-FLS-treated hamsters had

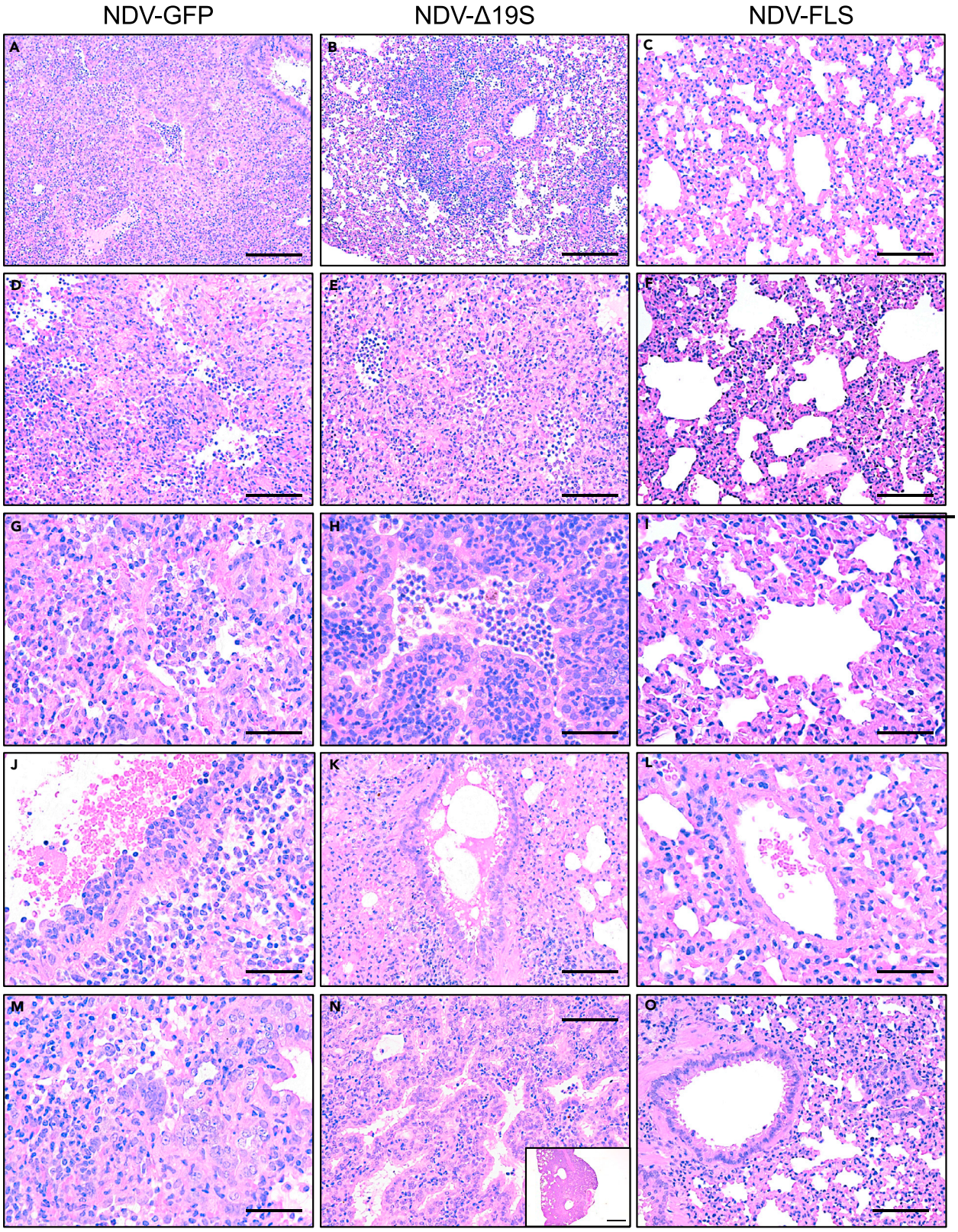
NDV-GFP
NDV-Δ19S
NDV-FLS
A
B
C
D
E
F
G
H
I
J
K
L
M
N
O

Figure 5. Histological analysis of pulmonary parenchyma from hamsters vaccinated (prime-boost schedule) with NDV-FLS, NDV-Δ19 and NDV-GFP, and challenged with SARS-CoV-2

For each treatment group (NDV-GFP, NDV-Δ19S, and NDV-FLS), the following are showed: inflammation within terminal bronchioles and alveoli (rows 1–3), inflammation around vessels and airways (row 4), and epithelial hyperplasia (row 5). At low magnification, no lesions are observed in the NDV-FLS-treated group (C), while lesions appear multifocal and diffuse in the NDV-Δ19S (B) and NDV-GFP (A) groups, respectively. Exudation of neutrophils, macrophages, and edema fluid is present in NDV-GFP- (D and G) and NDV-Δ19S- (E and H) treated hamsters, while NDV-FLS-treated hamsters showed no lesions (F and I). Perivascular and peribronchiolar inflammation, characterized by edema, mononuclear cells and scattered neutrophils is observed in NDV-GFP (J) and NDV-Δ19S (K) groups but not in the NDV-FLS group (L). Proliferation of mature type II pneumocytes (M) and bronchiolar epithelial cells (N) is observed in both NDV-Δ19S and NDV-GFP groups but not in the NDV-FLS group (O). The inset shows a subgross picture showing an area of marked epithelial hyperplasia. For figures A and B, bar = 200 μm; for figures C-F, K, N, O, bar = 100 μm; for figures G-J, L, M, bar = 50 μm. Inset, bar = 1 mm.

significantly less extensive areas of lung pathology compared with the NDV-Δ19S-, but not the NDV-GFP-treated group (Figure 4D). In the prime-boost cohort, the mean compound nominal score was significantly lower in NDV-FLS-treated hamsters compared to those in the NDV-GFP group; differences were not significant between the scores of the NDV-Δ19S- and the NDV-GFP- or NDV-FLS-treated groups (Figure 4E). Lastly, NDV-GFP- and NDV-Δ19S-treated hamsters had the highest extent of lesions, with five of six and three of six animals showing >50% of lung tissue affected, respectively; while in the NDV-FLS-treated group no hamsters had lesions in >50% of lung sections (Table S3). The average affected area scores were significantly different between NDV-FLS-treated hamsters and those in the NDV-GFP-treated group (Figure 4F).

In the prime-boost experiment, all hamsters treated with NDV-GFP presented with severe exudative lesions characterized by accumulation of sloughed cells, macrophages and neutrophils within the alveolar spaces, variably admixed with multifocal areas of hemorrhage and edema (Figures 5A, 5D, and 5G). In every hamster of this group, most bronchioles were filled with cellular debris and neutrophils. The connective tissues surrounding vessels and bronchioles was markedly expanded by edema and populated by inflammatory cells, such as macrophages, lymphocytes, fewer plasma cells, and scattered neutrophils. In all six hamsters, medium-size vessels showed segmental hyperplasia of the endothelial cells and sub-intimal accumulation of inflammatory cells, although no thrombosis was observed (Figure 5J). As animals were euthanized at day five pi, subacute changes were also observed, which included type II cell hyperplasia (Figure 5M), and presence of hemosiderin-laden macrophages mainly around the terminal bronchioles. In hamsters vaccinated with NDV-Δ19S (Figures 5B, 5E, 5H, 5K, and 5N), lesions were similar to the NDV-GFP-treated group, although the exudative changes were less prominent, noticeably with decreased amounts of desquamated cells in the alveolar spaces and bronchioles. In this group, most hamsters presented with numerous hemosiderin-laden macrophages (suggesting resolving hemorrhage) either in the alveoli or around bronchioles, type II cell hyperplasia (six of six hamsters), and marked hyperplasia of the bronchiolar epithelium in three of six hamsters (Figure 5N). In hamsters vaccinated with NDV-FLS, only two of six hamsters showed mild exudation of neutrophils in the alveoli, and only two presented with multifocal haemorrhages. Most of the lung parenchyma was unaffected (Figures 5C, 5F, 5I, 5L, and 5O). The other changes were subacute, including mild hyperplasia of type II cells (four of six hamsters), , and accumulation of hemosiderin-laden macrophages in four hamsters.

At the time of euthanasia, we also evaluated a series of hematological and serum chemistry parameters to test whether prime-boost vaccination could prevent any hematological changes upon infection of hamsters with SARS-CoV-2. All parameters were within normal limits and no clear trends emerged between vaccinated and control hamsters. Of note, NDV-GFP-vaccinated hamsters showed an elevated neutrophils count, and a higher neutrophil:lymphocyte ratio compared with those that were vaccinated with NDV-FLS, which has been correlated with disease severity in SARS-CoV-2-infected people (Karimi Shahri et al., 2020). This is consistent with the results of microscopic pathology, which showed numerous neutrophils into the lung of NDV-GFP-vaccinated hamsters.

Vaccination of hamsters with NDV vectors expressing SARS-CoV-2 S decreases the magnitude of SARS-CoV-2 replication in tissues

To evaluate the extent of virus replication in tissues, we quantified the presence of SARS-CoV-2 genomic RNA and infectious titers in the tissues of hamsters euthanized on day five pi. In the single-dose group, SARS-CoV-2 genome copy numbers were reduced significantly in the proximal and distal lungs of the NDV-FLS-treated group, while genome copies remained high in the hamsters treated with NDV-Δ19S and were not significantly different compared with controls (Figure 6A). Viral RNA levels in the nasal turbinates, small intestine, and blood did not differ between groups that received a single vaccine dose.

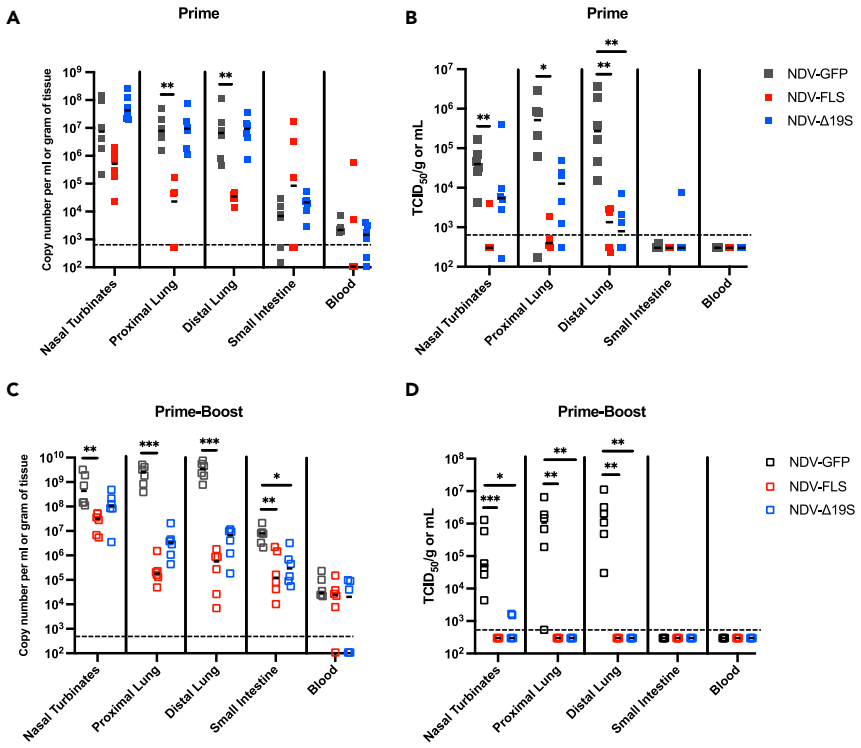

Figure 6. Magnitude of SARS-CoV-2 replication in tissues of vaccinated hamsters

Upon euthanasia at day 5 days post-infection (pi), RNA levels (A and C) and infectious titers (B and D) for SARS-CoV-2 were evaluated in hamsters vaccinated with a prime only (A and B) or prime-boost schedule (C and D). Viral RNA levels are reported as genome copy number, and virus titers are reported as mean tissue culture infectious dose ($TCID_{50}$). Shown are data scatterplot with medians (n = 6/group). The limits of detection are indicated with dashed lines. Differences in the magnitude of virus copy number or infectious titers were assessed by Kruskall-Wallis test with Dunn's test for multiple comparisons. * = <0.05, ** = <0.01, *** = <0.001.

Similarly, a single dose of NDV-FLS significantly reduced the titers of infectious SARS-CoV-2 in the nasal turbinates, proximal, and distal lungs, compared with the NDV-GFP control. The NDV-Δ19S-vaccinated hamsters only had significantly reduced viral titers in the distal lung (Figure 6B). This may be due to some partial protection that prevented the spread of virus into the lower lung.

In animals receiving two vaccine doses, the NDV-FLS group had significantly reduced SARS-CoV-2 genome copies in all tissues examined, except for blood. While the NDV-Δ19S-vaccinated hamsters only had significantly reduced viral RNA levels in the small intestine (Figure 6C), there was a clear trend toward lower viral RNA levels in both the proximal and distal lung (Figure 6C). Hamsters in both prime-boost vaccine groups did not have any infectious virus in the lungs, and only two animals had low levels of virus in the nasal turbinates, suggesting protection of both the upper and lower airway is provided by two vaccine doses (Figure 6D).

We also examined SARS-CoV-2 mucosal shedding following infection with SARS-CoV-2, since a key question regarding the protective efficacy of vaccination and whether vaccination can effectively prevent virus transmission. Oral and rectal swabs were sampled day 2 pi to test whether vaccination may prevent acute virus shedding by these routes. Viral RNA was detected in oral and rectal swabs in all hamsters regardless of the vaccine regimen, without differences in the magnitude of shedding between groups (Figure S1A). Quantification of infectious titers in swabs showed that most hamsters shed at very low levels ($<10^2$ $TCID_{50}$/ml) in both groups, and no differences were observed in the magnitude of shedding (Figure S1B) or the proportion of shedding compared with non-shedding animals (Fisher's exact test, data not show). This suggests that vaccination did not prevent infection and that virus shedding occurred in the early phases of infection, despite protection from disease. Whether the low levels of infectious virus in the oral and rectal swabs are sufficient to infect other hamsters is a question that remains to be answered.

Our data suggest that while vaccination prevented disease and significantly reduced viral growth in the tissues, infected animals may shed virus acutely after infection.

Differential expression of immune response related genes in vaccinated hamsters

To characterize the molecular drivers of inflammation and immune response in vaccinated and non-vaccinated hamsters, we examined the mRNA expression of various immune response-related genes (n = 11) in the lungs of hamsters in the prime-boost experimental groups, at day 5 pi. While several examined genes showed significant difference between vaccinated and control groups, only expression of interleukin (IL)-1β was significantly upregulated in both vaccine groups compared with the control (Figure S3). Vascular endothelial growth factor (VEGF) expression was the other and only gene to be upregulated in the NDV-FLS-treated group compared with the NDV-GFP control (Figure S3). The NDV-Δ19S-treated group showed differential expression of five additional genes compared with the NDV-GFP-treated control group: IL-6, FoxP3, IL-4, transforming growth factor (TGF)-β, and tumor necrosis factor alpha (TNF)-α (Figure S6). Upregulation of cytokine gene expression in vaccinated hamsters may account also for activation of the immune response, rather than tissue damage or inflammation, as pathology shows more severe lesions in the control (NDV-GFP) group.

We also examined relative expression levels of interferon gamma (IFN-γ) and IL-4 to attempt to determine whether a T helper type 1 (Th1) or Th2-associated bias in immune responses between groups may be driving susceptibility to infection. Both vaccine groups had higher, albeit not statistically significant, median IFN-γ:IL-4, ratios, and it is possible that inducing a Th1-associated immune response via vaccination may lead to improved infection outcomes (Jeyanathan et al., 2020).

Lyophilized NDV-FLS retains its infectivity

Given that hamsters vaccinated with NDV-FLS were protected from clinical signs and lesions following SARS-CoV-2 challenge, we sought to investigate whether it would be feasible to lyophilize this promising vaccine candidate thereby greatly simplifying its storage and distribution requirements. Aliquots of NDV-FLS stock containing the same number of PFU were adjusted to a final concentration of 5% sucrose, 5% sucrose/5% iodixanol, or mixed 1:1 with a solution containing 10% lactose, 2% peptone, 10mM Tris-HCl, pH 7.6, and lyophilized for 16h at −52°C. Two days later, samples were reconstituted in phosphate-buffered saline with 5% sucrose at the same volume and virus titer determined. As shown in Figure 7A, there was a ∼2 fold loss of infectivity when NDV-FLS was lyophilized in 10% lactose, 2% peptone, 10mM Tris-HCl, pH 7.6 compared with virus frozen at −70°C. Further, as shown by Western blot analysis, the reconstituted vaccine preparation contained S protein at amounts comparable with the purified virus stock maintained at ultracold temperature, and was able to infect and induce expression of S protein in DF-1 cells (Figure 7B). Given the convenience and greatly simplified storage and transportation requirements of a lyophilized vaccine, further optimization of the lyophilization conditions, as well as assessment of retained efficacy in challenge experiments, is warranted for NDV-based vaccines against SARS-CoV-2.

DISCUSSION

The COVID-19 pandemic has seen an unprecedented number of vaccine candidates, with as many as 14 approved for use in at least one country (Organization). Given the evolution of novel variants of concern (Kirola, 2021; van Oosterhout et al., 2021), the likelihood of persistent spread of SARS-CoV-2 for several years (Scudellari, 2020), emerging data which suggest that the Delta variant may spread more readily than other SARS-CoV-2 variants among people vaccinated against COVID-19 (Brown et al., 2021; Musser et al., 2021; Riemersma et al., 2021), limitations in production capacity of developed vaccines (Khamsi, 2020), and the need for evidence of efficacy for multiple platforms moving forward, there will be a need for a diverse set of vaccine candidates to advance through all stages of development. Here we tested two live vaccine candidates based on an NDV vector expressing SARS-CoV-2 spike protein or a truncated version of the same protein in a hamster model to assess their potential for prevention of COVID-19.

The Syrian hamster has been used by our and other groups as a robust model for SARS-CoV-2 infection, and it is used to examine viral pathogenesis as well as testing vaccine efficacy (Griffin et al., 2021; Muñoz-Fontela et al., 2020). We vaccinated groups of ten hamsters with either NDV vaccine candidate, or NDV expressing GFP as a negative control. The vaccines were administered either as a single dose or as

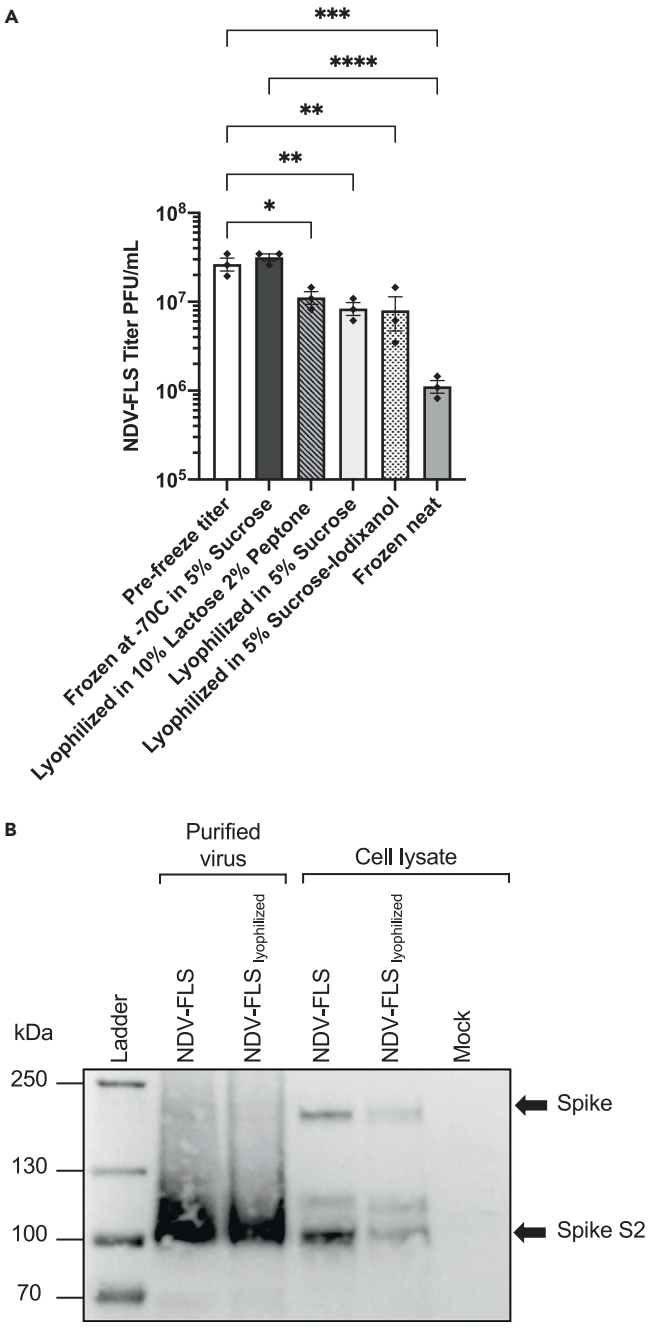

Figure 7. Lyophilized NDV-FLS virus retains infectivity

(A) Triplicate aliquots of equal numbers of NDV-FLS plaque-forming units (PFU) were either immediately frozen at −70°C or adjusted to a final concentration of 5% sucrose, 5% sucrose/5% Iodixanol, or mixed 1:1 with a stabilizing agent comprised of 10% lactose, 2% peptone, 10mM Tris-HCl, pH 7.6 and lyophilized at 44 x 10-3 MBAR and −52°C for 16 h. Lyophilized samples were stored at 4°C for 48 h before being resuspended in 1mL 5% sucrose/PBS and titered by mean tissue culture infectious dose ($TCID_{50}$) in DF-1 cells. Shown are data averages +/− SD (n = 3/group). Statistical analysis was by one-way analysis of variance (ANOVA) with Tukey's test for multiple comparisons. * = <0.05, ** = <0.01, *** = <0.001. (B) The lyophilized and reconstituted NDV-FLS (10% lactose and 2% peptone preparation) contains similar levels of Spike (S) protein compared to the purified virus stored at −70°C, as assessed by Western blot analysis when equal amounts of virus are loaded on the gel (10^7 PFU). Lyophilized and reconstituted NDV-FLS (10% lactose and 2% peptone preparation) expresses S protein in DF-1 cells at similar levels compared to NDV-FLS stored at −70°C, as assessed by Western blot of lysates from DF-1 infected with the same multiplicity of infection (MOI = 0.5).

two homologous doses 28 days apart. Both vaccines expressing SARS-CoV-2 S protein were immunogenic as assessed by ELISA for anti-SARS-CoV-2 IgG. Neither vaccine induced significantly high IgG titers after a single dose; however, following homologous booster immunization, both vaccine groups had significantly higher antibody titers compared with controls. When evaluating a prime-boost vaccination schedule, the vaccine expressing full-length S protein induced neutralizing antibody responses that were significantly greater than those seen in the group that received the vaccine with the truncated S protein. It is possible the low incorporation of the Δ19S into the NDV virion might have compromised an effective immune response due to lack of surface antigen presentation, despite the fact that NDV-Δ19S appeared to express higher amounts of S protein *in vitro*. Nonetheless, even the vaccine expressing the full-length S protein induced only modest $PRNT_{90}$ titers, suggesting that efficacy to protect from clinical disease and microscopic pathology may not be entirely dependent upon the magnitude of neutralizing antibody titers. Similarly, hamsters in the prime-boost NDV-Δ19S group appeared to be nearly fully protected from SARS-CoV-2 replication in the lungs, where no infectious titers were evident, despite barely detectable neutralizing antibodies and modest IgG serum titers. It is possible that protection following vaccination with NDV may also rely on T cell responses, which might have been more strongly activated by the NDV-Δ19S vaccine, as it expresses higher level of S protein upon infection. However, this was not examined in our study due to a lack of appropriate reagents, such as hamster-specific antibodies for flow cytometry and depletion studies. Overall, these data suggest that some protection against disease and decreased viral replication can be afforded in the absence of high titers of neutralizing antibodies and further characterization of the immune responses generated by NDV-vectored vaccines, and others will be critical for enhanced immunization strategies.

Treatment with either NDV vaccine was able to decrease or eliminate SARS-CoV-2 replication in the lungs of infected hamsters. Hamsters that received a single vaccine dose had only modest reductions in viral loads in the upper and lower airways but vaccination with NDV-FLS afforded significant decrease in virus titers with only one dose. In the prime-boost cohort, aside from two hamsters with low levels of detectable virus in the nasal turbinates (NDV-Δ19S group), infectious virus could not be detected in the airways of vaccinated hamsters. Consistent with previous findings, there were still high levels of viral RNA in tissues of infected animals, even in the absence of detectable virus. This is likely due to detection of subgenomic mRNA, intermediates of genomic replication, or the presence of intact degraded non-viable viral particles in long-lived phagocytic cells such as macrophages and dendritic cells.

While vaccination with a prime-boost regimen induced near sterilizing immunity in the airways at day 5 pi, detection of viral RNA and infectious virus at day 2 pi in the oral and rectal swabs from all groups (i.e., regardless of regimen) suggests the possibility that vaccination does not eliminate viral shedding during the acute stages of infection. However, on day 5 pi, when we collected tissues rather than swabs, we did not detect any replicating virus in tissues that would lead to shedding suggesting that the vaccine prevented shedding at this time point. This is in line with evidence gathered from the ongoing vaccination campaign, showing that infection and shedding in vaccinated people does occur and is related to the levels of antibody titers in blood, despite still proving highly effective against clinical disease (Bergwerk et al., 2021; Brown et al., 2021). Nonetheless, our data show that vaccination with an NDV vector provides clear protection against SARS-CoV-2 replication and establishment in the airways and lungs.

In the monodose schedule, NDV-FLS-vaccinated hamsters had mildly decreased severity and distribution of microscopic lesions compared with the NDV-Δ19S- and NDV-GFP-treated groups, although differences with the latter were not statistically significant. These results agree with the findings of virus titration in organs, which showed that the vaccines administered as a monodose did not confer sterilizing immunity and still afforded virus replication. In the prime-boost schedule, the severity and extent of microscopic lesions stratified the treatment groups consistently with the magnitude of serum neutralizing antibodies and levels of SARS-CoV-2 replication in lungs. Hamsters vaccinated with NDV-FLS showed no to minimal lesions, some of which (*i.e.*, epithelial hyperplasia and hemosiderophages) suggested that they were in the healing phase of the disease, without the presence of exudate. Hamsters treated with NDV-GFP showed the most severe lesions, characterized by presence of exudate in the alveoli and bronchioles. Finally, hamsters treated with NDV-Δ19S had lesions slightly less severe in extent and severity to those in the NDV-GFP group, albeit these differences were not statistically significant. Taken together, the pathology data indicate that NDV-FLS had a high protective effect against development of SARS-CoV-2-induced lesions, while NDV-Δ19S did so only partially.

Overall, the microscopic lesions caused by SARS-CoV-2 in the hamsters were consistent with the pathology documented elsewhere with this animal model (Chan et al., 2020a; Sia et al., 2020). The lesions observed in the control group (NDV-GFP) are also similar to what we observed in another pathogenesis study conducted by our team using untreated/naive hamsters (Griffin et al., 2021), indicating that the NDV backbone does not significantly affect the severity of SARS-CoV-2 infection in the lung. Lastly, development of hyaline membranes and marked fibrin exudation were not observed in our study. Although this is a typical feature of SARS-CoV-2 pathology in humans, this lesion has not been reported consistently in experimental settings (Gruber et al., 2020). Similarly, our model recapitulated development of vascular damage (*i.e.*, endothelialitis); however no thrombosis was observed (Gruber et al., 2020).

The protection from pulmonary lesions reflects abated clinical signs, as shown by the overall and mean weight loss differences between vaccinated and control hamsters, especially in the single-dose group. In the prime-boost group, while NDV-FLS protected from acute weight loss at 5 dpi, the control group out-paced NDV-FLS-vaccinated hamsters at later time points, up to the end of the experiment (day 28 pi). This could be partly explained by sampling artifact, caused by euthanizing animals with greater clinical signs first, and leaving less affected hamsters for long-term weight assessment. Alternatively, it is possible that hamster suffering a more severe disease (i.e., control group) may undergo a compensatory weight gain phase. This has been also observed by our group in a recent COVID-19 pathogenesis study that used a similar hamster model (Griffin et al., 2021).

Findings from the vaccination experiment unquestionably show that NDV-FLS is superior to NDV-Δ19S as a vaccine candidate against COVID-19. This suggests that incorporation of the vaccine antigen within the envelope of the NDV virion is necessary to trigger an effective immune response, possibly by direct interaction with B cell receptors as a prerequisite for induction of antibody responses (Heesters et al., 2016). While NDV-Δ19S-infected cells expressed higher levels of S protein compared with NDV-FLS-infected cells, the truncated S protein was poorly incorporated in the NDV envelope, as shown by Western blot analysis of purified vaccine preparations. While truncation of the 19 carboxy-terminal amino acids of the S protein has been shown to increase envelope incorporation in other viruses, such as VSV and lentiviral particles (Duan et al., 2020), this was not the case for NDV. This occurrence may be caused by a spatial mismatch between localization of the truncated S protein on the plasma membrane and specific sites of NDV release, which are cholesterol-rich sites defined as lipid rafts (Laliberte et al., 2006). Alternatively, truncation of the S protein may have led to inappropriate interaction with the NDV matrix (M) protein, which binds electrostatically with the NDV surface glycoproteins and drives budding of mature virions (Battisti et al., 2012; García-Sastre et al., 1989). This finding indicates that decoration of the vaccine envelope with the antigen of interest can improve the efficacy of vaccination, and further suggests that for development of NDV-based vaccine platforms, foreign surface epitopes should be chimerized with the transmembrane and cytoplasmic domains of NDV surface proteins (Sun et al., 2020a).

Several biomarkers of disease have been defined in COVID-19 patients, including changes in the concentration of cells in blood and in the presence of various cytokines and vascular growth factors (Karimi Shahri et al., 2020). In this study, we examined whether any significant hematological or serum chemistry changes could be detected and whether these might be indicative of disease progression, compared with protection against disease in prime-boost vaccinated animals. We detected elevated neutrophil counts as well as neutrophil:lymphocyte ratios in the blood of control hamsters, which have been linked to more severe disease progression (Li et al., 2020b). Specifically, neutrophilia appears to be induced by inflammatory mediators produced in diseased tissues, such as lung, and lymphopenia is a typical feature of acute viral infection, such as SARS-CoV-2 (Frater et al., 2020; Karimi Shahri et al., 2020). In the NDV-GFP-treated group, numerous neutrophils were recruited in the areas of affected lung, suggesting that neutrophilia was needed to satisfy peripheral tissue demands during infection. Elevated hemoglobin levels seen in control hamsters could also indicate some level of pulmonary distress and greater need for oxygen throughout the body, although in human patients low levels of hemoglobin appear to be associated with a poor outcome (Karimi Shahri et al., 2020). While some differences were seen in serum biomarkers such as glucose, urea nitrogen, and calcium, along with the above-mentioned changes in hematological markers, it is not possible to interpret the kinetics of these parameters with only one data point available.

Acute SARS-CoV-2 infection in hamsters lasts about one week, with a peak of infection between days two and four, therefore critical questions regarding viral replication and the immune responses generated may require

examination of animals euthanized at multiple time points. Accordingly, our examination of differentially expressed immune-related genes at day 5 pi represents a snapshot of one time point. Overall, our data show a trend by which cytokines appear to be more expressed in the lungs of vaccinated and challenged hamsters, compared to the control group, possibly as an effect of immune response activation. These differences appear to be more obvious in the NDV-Δ19S-vaccinated group, and may reflect the high levels of S protein expression seen *in vitro*. Conceivably, production of large amounts of intracellular foreign epitope may have triggered a more robust cell-mediated response compared to NDV-FLS, which induces lower S protein expression *in vitro* despite incorporating more S protein onto the envelope. Depletion studies could help define the contribution of cell-mediated and humoral response in the immunity elicited by our vaccines, however, lack of suitable reagents in hamsters limited our study to examining antibody responses and cytokine gene expression levels. Further characterization of immune responses and protective efficacy of NDV vaccines in other models such as mice or non-human primates may provide further insights into what immunological effector mechanisms are induced by vaccination with NDV and how these play a role in protection from disease.

Recombinant NDV vaccine platforms provide an option that has proven to be safe and immunogenic in several studies (Bukreyev et al., 2005; DiNapoli et al., 2007, 2010; Kim and Samal, 2016), and here is shown to provide full protection in a hamster model of COVID-19. Overall, the vaccines tested in this study were safe in hamsters, and expression of the S protein did not appear to change the virulence of the backbone. The vaccines were lentogenic (*i.e.*, non-virulent) in chicken eggs, consistent with a non-virulent fusion cleavage site of the NDV fusion protein (Cattoli et al., 2011), and were not neutralized by S protein-specific serum, suggesting that the S protein did not contribute to infectivity of NDV recombinants. Moreover, lyophilization of the NDV-FLS vaccine did not substantially reduce virus titer and maintained its ability to infect cells and express the S protein. Although these are attractive analytical qualities, the lyophilized and reconstituted NDV-FLS should be further tested in vaccination/challenge studies, to conclusively demonstrate retained immunogenicity upon lyophilization.

Despite having substantial incorporation of S protein in the envelope, NDV-FLS had lower fusogenic activity compared with NDV-Δ19S or NDV-GFP. The higher fusogenicity of NDV-Δ19S compared with NDV-FLS is likely mediated by the higher expression of truncated spike protein, as seen in DF-1 cells, and its increased localization on the plasma membrane, due to lack of the Golgi anchoring signal (Boson et al., 2021). Nonetheless, the ability of NDV-Δ19S to develop syncytia was similar to what observed with NDV-GFP, and did not increase virulence for embryonated eggs.

Recently, a live attenuated NDV vaccine against COVID-19 has been developed by another group. This vaccine was engineered to express either a wild-type spike protein, or a stabilized version that does not undergo cleavage (pre-fusion stabilized) (Sun et al., 2020a). Upon intramuscular delivery using 10–50 μg of purified virus preparation (virus was not quantified by an infectivity assay) in a homologous prime-boost schedule 21 days apart, both vaccines induced neutralizing antibody and completely inhibited replication of a mouse-adapted SARS-CoV-2 strain in the lungs of BALB/c mice. While this is similar to what was observed with our NDV-FLS prime-boost group, it should be noted that in mice, titers of SARS-CoV-2 in lung tissues peaked at approximately 10^4 PFU/lung lobe, as opposed to titers of up to 10^7 $TCID_{50}$/g of lung in the control hamsters of our study. Similarly, mice did not develop clinical signs or microscopic lesions, preventing assessment of protection against clinical signs or tissue damage (Sun et al., 2020a). An inactivated version of the same vaccine (10 μg alone or 5 μg with adjuvant) was also administered intramuscularly in an homologous prime-boost regimen, and it protected both mice and hamsters from virus replication in lung tissues at day 5 pi; however, microscopic lung pathology was not assessed in this research (Sun et al., 2020b). While these studies support the notion that NDV is a successful and versatile vaccine platform against SARS-CoV-2, differences regarding vaccine type (inactivated vs. infectious), delivery (intranasal vs. intramuscular), dose assessment (mass vs. infectivity), and type of animal model prevent a direct comparison with our results.

As NDV is a respiratory virus, in our vaccine trial we opted to deliver NDV intranasally, as already successfully attempted in other studies (Bukreyev et al., 2005; DiNapoli et al., 2007, 2010). Activation of the local mucosa-associated lymphoid tissue has the potential to markedly decrease nasal shedding of the virus (Gallo et al., 2021), which is of paramount importance to curtail circulation of SARS-CoV-2 in a partially immune population, and therefore limit the development of vaccine escape variants. Notably, in mice, complete protection against SARS-CoV-1 challenge is afforded only upon intranasal, but not subcutaneous, vaccine administration

(Zhao et al., 2016). Although in our study we did not test development of SARS-CoV-2-specific mucosal immunity due to lack of reagents, in the prime-boost schedule NDV-FLS-treated hamsters had no detectable infectious SARS-CoV-2 in the turbinates or the upper and lower lungs day 5 pi, suggesting development of sterilizing immunity. However, considering that low-level shedding of infectious virus was observed at day 2 pi even in vaccinated groups, vaccination may not protect against the early phases of SARS-CoV-2 replication. It is unclear if such low amounts of infectious virus would be able to infect other animals, or even if the detected virus may – at least in part – represent left-over inoculum. Lastly, as the prime-boost group in our study showed a clear increase of S-specific antibodies after the second dose, it is likely that immunity against the vector backbone did not impact the efficacy of a booster shot.

Many COVID-19 vaccine candidates are in various stages of clinical development, with some currently being given emergency-use approval in several countries. However, due to the relative advantages and disadvantages of different vaccine platforms, there is an ongoing need to develop and test novel vaccine platforms and strategies. This will also be critical in the case of potential future pandemics and emerging and re-emerging infections, which will require swift development of vaccine candidates. The prospect of having several different platforms available for rapid development should a novel pathogen arise is of critical importance. Live viral vectors are particularly advantageous due to their generally high immunogenicity, ability to induce both humoral and cellular immune responses, and the lack of a need for adjuvants (Vrba et al., 2020). This work provides evidence that this platform can provide substantial protection against SARS-CoV-2 infection and could be a viable option for further clinical development.

Limitations of the study

Oral and rectal swabs were taken on day two post-challenge with SARS-CoV-2 primarily to confirm viral replication in our hamster infection model; therefore, we did not take swabs on day five post-challenge. As these swabs were taken at such an acute time point, we cannot know for certain whether the virus or RNA detected was from leftover inoculum, at least in the oral swabs. Additionally, although the vaccine was administered to hamsters intranasally, the method of administration used would have resulted in vaccine reaching the distal lungs, where it could potentially replicate. To evaluate the true potential of intranasal administration of an NDV-based COVID-19 vaccine, a larger animal model such as a sheep, in which the efficacy of intranasal administration could be evaluated separate from pulmonary administration, would be required. Indeed, large animal studies to address efficacy of intranasal vs. pulmonary administration are currently ongoing.

STAR★METHODS

Detailed methods are provided in the online version of this paper and include the following:

- KEY RESOURCES TABLE
- RESOURCE AVAILABILITY
  - Lead contact
  - Materials availability
  - Data and code availability
- EXPERIMENTAL MODEL AND SUBJECT DETAILS
  - Ethics statement
  - Cells
- METHOD DETAILS
  - Engineering and rescue of recombinant NDV vaccines
  - Challenge virus and vaccine candidates
  - Immunofluorescence assay and titration of recombinant NDV vaccines
  - Vaccine characterization in DF-1 cells
  - Sodium dodecyl-sulfate polyacrylamide gel electrophoresis (SDS-PAGE) and western blot analysis
  - Neutralization of pseudotyped lentiviruses and NDV recombinant vaccines
  - Determination of mean death time (MDT)
  - Lyophilization of NDV-FLS
  - Immunization and infection of Syrian hamsters
  - Microscopic pathology
  - Detection of SARS-CoV-2 RNA in tissues and swabs of infected hamsters
  - Detection of infectious SARS-CoV-2 in tissues and swabs of infected hamsters
  - Determination of antibody responses by ELISA and PRNT assay

- Hematological and biochemical analysis of blood and serum
- Cytokine mRNA analysis
- QUANTIFICATION AND STATISTICAL ANALYSIS

SUPPLEMENTAL INFORMATION

Supplemental information can be found online at https://doi.org/10.1016/j.isci.2021.103219.

ACKNOWLEDGMENTS

This work was funded by an Ontario Ministry of Colleges and Universities COVID-19 Rapid Research Fund project grant to BWB, SKW, LS and DK (C-018-2415020-BRIDLE), the University of Guelph COVID-19 Research Development and Catalyst Fund granted to BWB, SKW, and LS, Natural Sciences and Engineering Research Council of Canada Discovery Grants to SKW (grant # 304737), LS (grant #401127) and BWB (grant #436264) and the Canadian Scientific Research and Experimental Development (SRED) program. The funders had no role in study design, data collection and analysis, decision to publish, or preparation of the manuscript. All work performed at the National Microbiology Laboratory was supported by the Public Health Agency of Canada.

AUTHOR CONTRIBUTIONS

Conceptualization, S.K.W., L.S., B.W.B, P.P.M., D.K., B.M.W., and B.D.G.; methodology, S.K.W., L.S., B.W.B., B.D.G., B.M.W., and D.K.; animal experiments (including vaccination, challenge, virus titration, and serology), B.M.W, M.C., R.V., N.T., E.V., A.L., S.H., B.D.G., J.A., M.H., K.T., A.A., K.L.F., and D.K., R.C.M, LC, Y.M., J.P.K., and J.A.M.; virus engineering and purification, L.A.S., Y.P., and J.G.E.Y.; vaccine characterization, A.L., P.H.P., and J.G.E.Y; microscopic pathology assessment, L.S; writing – original draft, B.M.W., S.K.W., L.S., and D.K.; funding acquisition and resources, B.W.B., S.K.W., L.S., and D.K.; supervision, S.K.W., L.S., B.W.B, D.K., L.B., D.S., H.W., and S.B.

DECLARATION OF INTERESTS

L.A.S., Y.P., B.W.B., P.P.M., L.S., and S.K.W. are co-inventors on a United States Provisional Application No. 63/196,489 entitled "ENGINEERED NEWCASTLE DISEASE VIRUS VECTOR AND USES THEREOF", which was filed June 3, 2021.

INCLUSION AND DIVERSITY

We worked to ensure sex balance in the selection of non-human subjects. One or more of the authors of this paper self-identifies as an underrepresented ethnic minority in science. One or more of the authors of this paper self-identifies as a member of the LGBTQ + community. One or more of the authors of this paper self-identifies as living with a disability. While citing references scientifically relevant for this work, we also actively worked to promote gender balance in our reference list.

Received: May 7, 2021
Revised: August 24, 2021
Accepted: September 30, 2021
Published: November 19, 2021

REFERENCES

Afonso, C.L. (2008). Not so fast on recombination analysis of Newcastle disease virus. J. Virol. *82*, 9303. https://doi.org/10.1128/JVI.01231-08.

Andersen, K.G., Rambaut, A., Lipkin, W.I., Holmes, E.C., and Garry, R.F. (2020). The proximal origin of SARS-CoV-2. Nat. Med. *26*, 450–452. https://doi.org/10.1038/s41591-020-0820-9.

Battisti, A.J., Meng, G., Winkler, D.C., McGinnes, L.W., Plevka, P., Steven, A.C., Morrison, T.G., and Rossmann, M.G. (2012). Structure and assembly of a paramyxovirus matrix protein. Proc. Natl. Acad. Sci. U S A *109*, 13996–14000. https://doi.org/10.1073/pnas.1210275109.

Bergwerk, M., Gonen, T., Lustig, Y., Amit, S., Lipsitch, M., Cohen, C., Mandelboim, M., Gal Levin, E., Rubin, C., Indenbaum, V., et al. (2021). Covid-19 breakthrough infections in vaccinated health Care workers. N. Engl. J. Med. https://doi.org/10.1056/NEJMoa2109072.

Besutti, G., Bonacini, R., Iotti, V., Marini, G., Riva, N., Dolci, G., Maiorana, M., Spaggiari, L., Monelli, F., Ligabue, G., et al. (2020). Abdominal visceral infarction in 3 patients with COVID-19. Emerg. Infect. Dis. *26*, 1926–1928. https://doi.org/10.3201/eid2608.201161.

Boson, B., Legros, V., Zhou, B., Siret, E., Mathieu, C., Cosset, F.L., Lavillette, D., and Denolly, S. (2021). The SARS-CoV-2 envelope and membrane proteins modulate maturation and retention of the spike protein, allowing assembly of virus-like particles. J. Biol. Chem. *296*, 100111. https://doi.org/10.1074/jbc.RA120.016175.

Bradley, B.T., Maioli, H., and Johnston, R. (2020). Histopathology and ultrastructural findings of

fatal COVID-19 infections in Washington State: a case series (vol 396, pg 320, 2020). Lancet *396*, 312.

Brown, C.M., Vostok, J., Johnson, H., Burns, M., Gharpure, R., Sami, S., Sabo, R.T., Hall, N., Foreman, A., Schubert, P.L., et al. (2021). Outbreak of SARS-CoV-2 infections, including COVID-19 vaccine breakthrough infections, associated with large public gatherings - barnstable county, Massachusetts, july 2021. MMWR Morb. Mortal. Wkly Rep. *70*, 1059–1062. https://doi.org/10.15585/mmwr.mm7031e2.

Bukreyev, A., Huang, Z., Yang, L., Elankumaran, S., St Claire, M., Murphy, B.R., Samal, S.K., and Collins, P.L. (2005). Recombinant newcastle disease virus expressing a foreign viral antigen is attenuated and highly immunogenic in primates. J. Virol. *79*, 13275–13284. https://doi.org/10.1128/JVI.79.21.13275-13284.2005.

Calabrese, F., Pezzuto, F., Fortarezza, F., Hofman, P., Kern, I., Panizo, A., von der Thusen, J., Timofeev, S., Gorkiewicz, G., and Lunardi, F. (2020). Pulmonary pathology and COVID-19: lessons from autopsy. The experience of European Pulmonary Pathologists. Virchows Arch. https://doi.org/10.1007/s00428-020-02886-6.

Calzas, C., and Chevalier, C. (2019). Innovative mucosal vaccine formulations against influenza A virus infections. Front. Immunol. *10*, 1605. https://doi.org/10.3389/fimmu.2019.01605.

Capua, I., and Alexander, D.J. (2004). Human health implications of avian influenza viruses and paramyxoviruses. Eur. J. Clin. Microbiol. Infect. Dis. *23*, 1–6. https://doi.org/10.1007/s10096-003-1059-3.

Cattoli, G., Susta, L., Terregino, C., and Brown, C. (2011). Newcastle disease: a review of field recognition and current methods of laboratory detection. J. Vet. Diagn. Invest. *23*, 637–656. https://doi.org/10.1177/1040638711407887.

Chan, J.F., Zhang, A.J., Yuan, S., Poon, V.K., Chan, C.C., Lee, A.C., Chan, W.M., Fan, Z., Tsoi, H.W., Wen, L., et al. (2020a). Simulation of the clinical and pathological manifestations of coronavirus disease 2019 (COVID-19) in a golden Syrian hamster model: implications for disease pathogenesis and transmissibility. Clin. Infect. Dis. *71*, 2428–2446. https://doi.org/10.1093/cid/ciaa325.

Chan, J.F.W., Yuan, S.F., Kok, K.H., To, K.K.W., Chu, H., Yang, J., Xing, F.F., Liu, J.L., Yip, C.C.Y., Poon, R.W.S., et al. (2020b). A familial cluster of pneumonia associated with the 2019 novel coronavirus indicating person-to-person transmission: a study of a family cluster. Lancet *395*, 514–523. https://doi.org/10.1016/S0140-6736(20)30154-9.

Csatary, L.K., Eckhardt, S., Bukosza, I., Czegledi, F., Fenyvesi, C., Gergely, P., Bodey, B., and Csatary, C.M. (1993). Attenuated veterinary virus vaccine for the treatment of cancer. Cancer Detect. Prev. *17*, 619–627.

DiNapoli, J.M., Yang, L., Suguitan, A., Jr., Elankumaran, S., Dorward, D.W., Murphy, B.R., Samal, S.K., Collins, P.L., and Bukreyev, A. (2007). Immunization of primates with a Newcastle disease virus-vectored vaccine via the respiratory tract induces a high titer of serum neutralizing antibodies against highly pathogenic avian influenza virus. J. Virol. *81*, 11560–11568. https://doi.org/10.1128/JVI.00713-07.

DiNapoli, J.M., Yang, L., Samal, S.K., Murphy, B.R., Collins, P.L., and Bukreyev, A. (2010). Respiratory tract immunization of non-human primates with a Newcastle disease virus-vectored vaccine candidate against Ebola virus elicits a neutralizing antibody response. Vaccine *29*, 17–25. https://doi.org/10.1016/j.vaccine.2010.10.024.

Domingo, P., Mur, I., Pomar, V., Corominas, H., Casademont, J., and de Benito, N. (2020). The four horsemen of a viral Apocalypse: the pathogenesis of SARS-CoV-2 infection (COVID-19). EBioMedicine *58*, 102887. https://doi.org/10.1016/j.ebiom.2020.102887.

Duan, L., Zheng, Q., Zhang, H., Niu, Y., Lou, Y., and Wang, H. (2020). The SARS-CoV-2 spike glycoprotein biosynthesis, structure, function, and antigenicity: implications for the design of spike-based vaccine immunogens. Front. Immunol. *11*, 576622. https://doi.org/10.3389/fimmu.2020.576622.

Frater, J.L., Zini, G., d'Onofrio, G., and Rogers, H.J. (2020). COVID-19 and the clinical hematology laboratory. Int. J. Lab. Hematol. *42* (*Suppl 1*), 11–18. https://doi.org/10.1111/ijlh.13229.

Frutos, R., Serra-Cobo, J., Chen, T., and Devaux, C.A. (2020). COVID-19: time to exonerate the pangolin from the transmission of SARS-CoV-2 to humans. Infect. Genet. Evol. *84*, 104493. https://doi.org/10.1016/j.meegid.2020.104493.

Fukushi, S., Mizutani, T., Saijo, M., Matsuyama, S., Miyajima, N., Taguchi, F., Itamura, S., Kurane, I., and Morikawa, S. (2005). Vesicular stomatitis virus pseudotyped with severe acute respiratory syndrome coronavirus spike protein. J. Gen. Virol. *86*, 2269–2274. https://doi.org/10.1099/vir.0.80955-0.

Gallo, O., Locatello, L.G., Mazzoni, A., Novelli, L., and Annunziato, F. (2021). The central role of the nasal microenvironment in the transmission, modulation, and clinical progression of SARS-CoV-2 infection. Mucosal Immunol. *14*, 305–316. https://doi.org/10.1038/s41385-020-00359-2.

García-Sastre, A., Cabezas, J.A., and Villar, E. (1989). Proteins of Newcastle disease virus envelope: interaction between the outer hemagglutinin-neuraminidase glycoprotein and the inner non-glycosylated matrix protein. Biochim. Biophys. Acta *999*, 171–175. https://doi.org/10.1016/0167-4838(89)90214-8.

Griffin, B.D., Chan, M., Tailor, N., Mendoza, E.J., Leung, A., Warner, B.M., Duggan, A.T., Moffat, E., He, S., Garnett, L., et al. (2020). North American Deer Mice Are Susceptible to SARS-CoV-2. bioRxiv. 2020.2007.2025.221291. https://doi.org/10.1101/2020.07.25.221291.

Griffin, B.D., Warner, B.M., Chan, M., Mendoza, E.J., Tailor, N., Banadyga, L., Leung, A., He, S., Boese, A.S., Audet, J., et al. (2021). Exposure route, sex, and age influence disease outcome in a golden Syrian hamster model of SARS-CoV-2 infection. bioRxiv, 448196. https://doi.org/10.1101/2021.06.12.448196.

Gruber, A.D., Osterrieder, N., Bertzbach, L.D., Vladimirova, D., Greuel, S., Ihlow, J., Horst, D., Trimpert, J., and Dietert, K. (2020). Standardization of reporting criteria for lung pathology in SARS-CoV-2-infected hamsters: what matters? Am. J. Respir. Cell Mol. Biol. *63*, 856–859. https://doi.org/10.1165/rcmb.2020-0280LE.

Heesters, B.A., van der Poel, C.E., Das, A., and Carroll, M.C. (2016). Antigen presentation to B cells. Trends Immunol. *37*, 844–854. https://doi.org/10.1016/j.it.2016.10.003.

Imai, M., Iwatsuki-Horimoto, K., Hatta, M., Loeber, S., Halfmann, P.J., Nakajima, N., Watanabe, T., Ujie, M., Takahashi, K., Ito, M., et al. (2020). Syrian hamsters as a small animal model for SARS-CoV-2 infection and countermeasure development. Proc. Natl. Acad. Sci. U S A *117*, 16587–16595. https://doi.org/10.1073/pnas.2009799117.

Ioannidis, J.P.A. (2021). Reconciling estimates of global spread and infection fatality rates of COVID-19: an overview of systematic evaluations. Eur. J. Clin. Invest. *51*, e13554. https://doi.org/10.1111/eci.13554.

Jeyanathan, M., Afkhami, S., Smaill, F., Miller, M.S., Lichty, B.D., and Xing, Z. (2020). Immunological considerations for COVID-19 vaccine strategies. Nat. Rev. Immunol. https://doi.org/10.1038/s41577-020-00434-6.

Johnson, M.C., Lyddon, T.D., Suarez, R., Salcedo, B., LePique, M., Graham, M., Ricana, C., Robinson, C., and Ritter, D.G. (2020). Optimized pseudotyping conditions for the SARS-COV-2 spike glycoprotein. J. Virol. *94*. https://doi.org/10.1128/JVI.01062-20.

Kandeil, A., Bagato, O., Zaraket, H., Debeauchamp, J., Krauss, S., El-Shesheny, R., Webby, R.J., Ali, M.A., and Kayali, G. (2014). Proteolytic enzymes in embryonated chicken eggs sustain the replication of egg-grown low-pathogenicity avian influenza viruses in cells in the absence of exogenous proteases. J. Virol. Methods *202*, 28–33. https://doi.org/10.1016/j.jviromet.2014.02.023.

Karadag, E. (2020). Increase in COVID-19 cases and case-fatality and case-recovery rates in Europe: a cross-temporal meta-analysis. J. Med. Virol. *92*, 1511–1517. https://doi.org/10.1002/jmv.26035.

Karber, G. (1931). Breitag zur kollektivenbehandlung pharmakologischer reihenversuche. Archiv fur ExperimentellePathologie und Pharmakologie *162*, 480–483.

Karimi Shahri, M., Niazkar, H.R., and Rad, F. (2020). COVID-19 and hematology findings based on the current evidences: a puzzle with many missing pieces. Int. J. Lab Hematol. https://doi.org/10.1111/ijlh.13412.

Khamsi, R. (2020). If a coronavirus vaccine arrives, can the world make enough? Nature *580*, 578–580. https://doi.org/10.1038/d41586-020-01063-8.

Kim, S.H., and Samal, S.K. (2016). Newcastle disease virus as a vaccine vector for development of human and veterinary vaccines. Viruses *8*. https://doi.org/10.3390/v8070183.

Kirola, L. (2021). Genetic emergence of B.1.617.2 in COVID-19. New Microbes New Infect. *43*, 100929. https://doi.org/10.1016/j.nmni.2021.100929.

Kolakofsky, D., Pelet, T., Garcin, D., Hausmann, S., Curran, J., and Roux, L. (1998). Paramyxovirus RNA synthesis and the requirement for hexamer genome length: the rule of six revisited. J. Virol. *72*, 891–899. https://doi.org/10.1128/JVI.72.2.891-899.1998.

Kupferschmidt, K. (2021). New mutations raise specter of 'immune escape. Science *371*, 329–330. https://doi.org/10.1126/science.371.6527.329.

Laliberte, J.P., McGinnes, L.W., Peeples, M.E., and Morrison, T.G. (2006). Integrity of membrane lipid rafts is necessary for the ordered assembly and release of infectious Newcastle disease virus particles. J. Virol. *80*, 10652–10662. https://doi.org/10.1128/JVI.01183-06.

Li, Q., Guan, X.H., Wu, P., Wang, X.Y., Zhou, L., Tong, Y.Q., Ren, R.Q., Leung, K.S.M., Lau, E.H.Y., Wong, J.Y., et al. (2020a). Early transmission dynamics in Wuhan, China, of novel coronavirus-infected pneumonia. N. Engl. J. Med. *382*, 1199–1207. https://doi.org/10.1056/NEJMoa2001316.

Li, X., Liu, C., Mao, Z., Xiao, M., Wang, L., Qi, S., and Zhou, F. (2020b). Predictive values of neutrophil-to-lymphocyte ratio on disease severity and mortality in COVID-19 patients: a systematic review and meta-analysis. Crit. Care *24*, 647. https://doi.org/10.1186/s13054-020-03374-8.

Liu, J.Y., Liao, X.J., Qian, S., Yuan, J., Wang, F.X., Liu, Y.X., Wang, Z.Q., Wang, F.S., Liu, L., and Zhang, Z. (2020). Community transmission of severe acute respiratory syndrome coronavirus 2, shenzhen, China, 2020. Emerg. Infect. Dis. *26*, 1320–1323. https://doi.org/10.3201/eid2606.200239.

Lu, R., Zhao, X., Li, J., Niu, P., Yang, B., Wu, H., Wang, W., Song, H., Huang, B., Zhu, N., et al. (2020). Genomic characterisation and epidemiology of 2019 novel coronavirus: implications for virus origins and receptor binding. Lancet *395*, 565–574. https://doi.org/10.1016/S0140-6736(20)30251-8.

Mallapaty, S. (2020). How deadly is the coronavirus? Scientists are close to an answer. Nature *582*, 467–468. https://doi.org/10.1038/d41586-020-01738-2.

Martines, R.B., Ritter, J.M., Matkovic, E., Gary, J., Bollweg, B.C., Bullock, H., Goldsmith, C.S., Silva-Flannery, L., Seixas, J.N., Reagan-Steiner, S., et al. (2020). Pathology and pathogenesis of SARS-CoV-2 associated with fatal coronavirus disease, United States. Emerg. Infect. Dis. *26*, 2005–2015. https://doi.org/10.3201/eid2609.202095.

McGinnes, L.W., Pantua, H., Reitter, J., and Morrison, T.G. (2006). Newcastle disease virus: propagation, quantification, and storage. Curr. Protoc. Microbiol. *15*, 15F.12. https://doi.org/10.1002/9780471729259.mc15f02s01.

Meyerholz, D.K., and Beck, A.P. (2020). Histopathologic evaluation and scoring of viral lung infection. Methods Mol. Biol. *2099*, 205–220. https://doi.org/10.1007/978-1-0716-0211-9_16.

Muñoz-Fontela, C., Dowling, W.E., Funnell, S.G.P., Gsell, P.S., Riveros-Balta, A.X., Albrecht, R.A., Andersen, H., Baric, R.S., Carroll, M.W., Cavaleri, M., et al. (2020). Animal models for COVID-19. Nature *586*, 509–515. https://doi.org/10.1038/s41586-020-2787-6.

Musser, J.M., Christensen, P.A., Olsen, R.J., Long, S.W., Subedi, S., Davis, J.J., Hodjat, P., Walley, D.R., Kinskey, J.C., and Gollihar, J. (2021). Delta variants of SARS-CoV-2 cause significantly increased vaccine breakthrough COVID-19 cases in Houston, Texas. medRxiv, 21260808. https://doi.org/10.1101/2021.07.19.21260808.

Ong, S.W.X., Tan, Y.K., Chia, P.Y., Lee, T.H., Ng, O.T., Wong, M.S.Y., and Marimuthu, K. (2020). Air, surface environmental, and personal protective equipment contamination by severe acute respiratory syndrome coronavirus 2 (SARS-CoV-2) from a symptomatic patient. JAMA *323*, 1610–1612. https://doi.org/10.1001/jama.2020.3227.

van Oosterhout, C., Hall, N., Ly, H., and Tyler, K.M. (2021). COVID-19 evolution during the pandemic - implications of new SARS-CoV-2 variants on disease control and public health policies. Virulence *12*, 507–508. https://doi.org/10.1080/21505594.2021.1877066.

Organization, W.H. (n.d.) Draft Landscape and Tracker of COVID-19 Candidate Vaccines. https://www.who.int/publications/m/item/draft-landscape-of-covid-19-candidate-vaccines.

Ou, X., Liu, Y., Lei, X., Li, P., Mi, D., Ren, L., Guo, L., Guo, R., Chen, T., Hu, J., et al. (2020). Characterization of spike glycoprotein of SARS-CoV-2 on virus entry and its immune cross-reactivity with SARS-CoV. Nat. Commun. *11*, 1620. https://doi.org/10.1038/s41467-020-15562-9.

Park, M.S., Steel, J., García-Sastre, A., Swayne, D., and Palese, P. (2006). Engineered viral vaccine constructs with dual specificity: avian influenza and Newcastle disease. Proc. Natl. Acad. Sci. U S A *103*, 8203–8208. https://doi.org/10.1073/pnas.0602566103.

Pecora, A.L., Rizvi, N., Cohen, G.I., Meropol, N.J., Sterman, D., Marshall, J.L., Goldberg, S., Gross, P., O'Neil, J.D., Groene, W.S., et al. (2002). Phase I trial of intravenous administration of PV701, an oncolytic virus, in patients with advanced solid cancers. J. Clin. Oncol. *20*, 2251–2266. https://doi.org/10.1200/JCO.2002.08.042.

Peiris, M., and Leung, G.M. (2020). What can we expect from first-generation COVID-19 vaccines? Lancet *396*, 1467–1469. https://doi.org/10.1016/S0140-6736(20)31976-0.

Pham, P.H., Leacy, A., Deng, L., Nagy, É., and Susta, L. (2020). Isolation of Ontario aquatic bird bornavirus 1 and characterization of its replication in immortalized avian cell lines. Virol. J. *17*, 16. https://doi.org/10.1186/s12985-020-1286-6.

Riemersma, K.K., Grogan, B.E., Kita-Yarbro, A., Halfmann, P., Kocharian, A., Florek, K.R., Westergaard, R., Bateman, A., Jeppson, G.E., Kawaoka, Y., et al. (2021). Shedding of infectious SARS-CoV-2 despite vaccination when the delta variant is prevalent - Wisconsin. medRxiv, 21261387. https://doi.org/10.1101/2021.07.31.21261387.

Rima, B., Balkema-Buschmann, A., Dundon, W.G., Duprex, P., Easton, A., Fouchier, R., Kurath, G., Lamb, R., Lee, B., Rota, P., et al. (2019). ICTV Virus Taxonomy Profile. Paramyxoviridae. J. Gen. Virol. *100*, 1593–1594.

Russell, T.W., Hellewell, J., Jarvis, C.I., van Zandvoort, K., Abbott, S., Ratnayake, R., Cmmid Covid-Working, G., Flasche, S., Eggo, R.M., Edmunds, W.J., and Kucharski, A.J. (2020). Estimating the infection and case fatality ratio for coronavirus disease (COVID-19) using age-adjusted data from the outbreak on the Diamond Princess cruise ship. Euro Surveill. *25*. https://doi.org/10.2807/1560-7917.ES.2020.25.12.2000256.

Santry, L.A., McAusland, T.M., Susta, L., Wood, G.A., Major, P.P., Petrik, J.J., Bridle, B.W., and Wootton, S.K. (2018). Production and purification of high-titer newcastle disease virus for use in preclinical mouse models of cancer. Mol. Ther. Methods Clin. Dev. *9*, 181–191. https://doi.org/10.1016/j.omtm.2017.10.004.

Scudellari, M. (2020). How the pandemic might play out in 2021 and beyond. Nature *584*, 22–25. https://doi.org/10.1038/d41586-020-02278-5.

Sergel, T.A., McGinnes, L.W., and Morrison, T.G. (2000). A single amino acid change in the Newcastle disease virus fusion protein alters the requirement for HN protein in fusion. J. Virol. *74*, 5101–5107.

Shirvani, E., and Samal, S.K. (2020). Newcastle disease virus as a vaccine vector for SARS-CoV-2. Pathogens *9*. https://doi.org/10.3390/pathogens9080619.

Sia, S.F., Yan, L.M., Chin, A.W.H., Fung, K., Choy, K.T., Wong, A.Y.L., Kaewpreedee, P., Perera, R.A.P.M., Poon, L.L.M., Nicholls, J.M., et al. (2020). Pathogenesis and transmission of SARS-CoV-2 in golden hamsters. Nature. https://doi.org/10.1038/s41586-020-2342-5.

Sun, W., Leist, S.R., McCroskery, S., Liu, Y., Slamanig, S., Oliva, J., Amanat, F., Schafer, A., Dinnon, K.H., 3rd, Garcia-Sastre, A., et al. (2020a). Newcastle disease virus (NDV) expressing the spike protein of SARS-CoV-2 as a live virus vaccine candidate. EBioMedicine *62*, 103132. https://doi.org/10.1016/j.ebiom.2020.103132.

Sun, W., McCroskery, S., Liu, W.C., Leist, S.R., Liu, Y., Albrecht, R.A., Slamanig, S., Oliva, J., Amanat, F., Schäfer, A., et al. (2020b). A newcastle disease virus (NDV) expressing a membrane-anchored spike as a cost-effective inactivated SARS-CoV-2 vaccine. Vaccines (Basel) *8*. https://doi.org/10.3390/vaccines8040771.

Varga, Z., Flammer, A.J., Steiger, P., Haberecker, M., Andermatt, R., Zinkernagel, A.S., Mehra, M.R., Schuepbach, R.A., Ruschitzka, F., and Moch, H. (2020). Endothelial cell infection and endotheliitis in COVID-19. Lancet *395*, 1417–1418. https://doi.org/10.1016/S0140-6736(20)30937-5.

Verity, R., Okell, L.C., Dorigatti, I., Winskill, P., Whittaker, C., Imai, N., Cuomo-Dannenburg, G., Thompson, H., Walker, P.G.T., Fu, H., et al. (2020). Estimates of the severity of coronavirus disease 2019: a model-based analysis. Lancet Infect. Dis. *20*, 669–677. https://doi.org/10.1016/S1473-3099(20)30243-7.

Vrba, S.M., Kirk, N.M., Brisse, M.E., Liang, Y., and Ly, H. (2020). Development and applications of

viral vectored vaccines to combat zoonotic and emerging public health threats. Vaccines *8*. https://doi.org/10.3390/vaccines8040680.

Warner, B.M., Safronetz, D., and Kobinger, G.P. (2017). Syrian hamsters as a small animal model for emerging infectious diseases: advances in immunologic methods. Adv. Exp. Med. Biol. *972*, 87–101. https://doi.org/10.1007/5584_2016_135.

Wheelock, E.F., and Dingle, J.H. (1964). Observations on the repeated administration of viruses to a patient with acute leukemia. A preliminary report. N. Engl. J. Med. *271*, 645–651. https://doi.org/10.1056/NEJM196409242711302.

WHO, (n.d.) (Last accessed 2020.09.07). WHO Coronavirus Disease (COVID-19) Dashboard. https://covid19.who.int.

Williamson, E.J., Walker, A.J., Bhaskaran, K., Bacon, S., Bates, C., Morton, C.E., Curtis, H.J., Mehrkar, A., Evans, D., Inglesby, P., et al. (2020). Factors associated with COVID-19-related death using OpenSAFELY. Nature. https://doi.org/10.1038/s41586-020-2521-4.

Zhao, W., Zhang, Z., Zsak, L., and Yu, Q. (2015). P and M gene junction is the optimal insertion site in Newcastle disease virus vaccine vector for foreign gene expression. J. Gen. Virol. *96*, 40–45. https://doi.org/10.1099/vir.0.068437-0.

Zhao, J., Zhao, J., Mangalam, A.K., Channappanavar, R., Fett, C., Meyerholz, D.K., Agnihothram, S., Baric, R.S., David, C.S., and Perlman, S. (2016). Airway memory CD4(+) T cells mediate protective immunity against emerging respiratory coronaviruses. Immunity *44*, 1379–1391. https://doi.org/10.1016/j.immuni.2016.05.006.

Zhou, P., Yang, X.L., Wang, X.G., Hu, B., Zhang, L., Zhang, W., Si, H.R., Zhu, Y., Li, B., Huang, C.L., et al. (2020). A pneumonia outbreak associated with a new coronavirus of probable bat origin. Nature *579*, 270–273. https://doi.org/10.1038/s41586-020-2012-7.

Ziegler, C.G.K., Allon, S.J., Nyquist, S.K., Mbano, I.M., Miao, V.N., Tzouanas, C.N., Cao, Y.M., Yousif, A.S., Bals, J., Hauser, B.M., et al. (2020). SARS-CoV-2 receptor ACE2 is an interferon-stimulated gene in human airway epithelial cells and is detected in specific cell subsets across tissues. Cell *181*, 1016. https://doi.org/10.1016/j.cell.2020.04.035.

El Zowalaty, M.E., and Jarhult, J.D. (2020). From SARS to COVID-19: a previously unknown SARS- related coronavirus (SARS-CoV-2) of pandemic potential infecting humans - call for a One Health approach. One Health *9*, 100124. https://doi.org/10.1016/j.onehlt.2020.100124.

STAR★METHODS

KEY RESOURCES TABLE

REAGENT or RESOURCE	SOURCE	IDENTIFIER
Antibodies		
Mouse anti-NDV ribonucleoprotein	Novus Biologicals	NBP2-11633
Goat anti-Mouse IgG conjugated to Alexa Fluor 488	ThermoFisher	Cat# A-11001; RRID:AB_2534069
Rabbit anti-SARS-CoV-2 nucleocapsid	ThermoFisher	Cat# PA5-81794; RRID:AB_2788968
Rabbit anti-SARS-CoV-2 S1	ThermoFisher	Cat# PA5-81795; RRID:AB_2788969
Rabbit anti-SARS-CoV-2 S2	Novus Biologicals	Cat# NB100-56578; RRID:AB_838846
Mouse anti-beta actin	ThermoFisher	Cat# MA5-15739; RRID:AB_10979409
Goat anti-rabbit IgG conjugated to horseradish peroxidase	ThermoFisher	Cat# G-21234; RRID:AB_2536530
Goat anti-mouse IgG conjugated to horseradish peroxidase	ThermoFisher	Cat# G-21040; RRID:AB_2536527
Goat anti-hamster IgG (H+L) conjugated to horseradish peroxidase	KPL	5220-0371
Bacterial and virus strains		
NEB® Stable Competent E. coli (High Efficiency)	New England Biolabs	C3040I
SARS-CoV-2; hCoV-19/Canada/ON-VIDO-01/2020, GISAID accession# EPI_ISL_425177	Sunnybrook Research Institute	NA
NDV-FLS	University of Guelph	NA
NDV-Δ19S	University of Guelph	NA
NDV-GFP	University of Guelph	NA
Chemicals, peptides, and recombinant proteins		
2.5% Trypsin (10X)	ThermoFisher	15090-046
Protease inhibitor cocktail	ThermoFisher	0087785
Pierce SuperSignal West Pico PLUS Chemiluminescent Substrate	ThermoFisher	34580
L-poly-L-lysine	Millipore Sigma	P4707
Iodixanol (OptiPrep™ Density Gradient Medium)	Millipore Sigma	D1556
Lactose	Millipore Sigma	17814
Peptone	Millipore Sigma	P6838
SARS-CoV-2 (2019-n-CoV) Spike protein (S1+S2 ECD, His Tag)	Sino Biological	40589-V08B1
SARS-CoV-2 (2019-nCoV) Nucleocapsid-His recombinant Protein	Sino Biological	40588-V08B
1 Step Ultra TMB-ELISA substrate	ThermoFisher	34028
Carboxymethylcellulose	Millipore Sigma	C5678
Crystal Violet, 0.5% Solution	Fisher	S25275B
10% neutral-buffered formalin	Fisher	22-220682
Critical commercial assays		
Pierce BCA Protein Assay Kit	ThermoFisher	23225
Pierce Firefly luciferase Glow Assay Kit	ThermoFisher	16176
QIAamp Viral RNA mini kit	Qiagen	52906
RLT Buffer	Qiagen	79216
RNeasy Plus Mini kit	Qiagen	74134
TaqPath 1-Step Multiplex Master Mix kit	ThermoFisher	A28525
Experimental models: Cell lines		
Vero	ATCC	CCL-81
Vero E6	ATCC	CRL-1586

(*Continued on next page*)

Continued

REAGENT or RESOURCE	SOURCE	IDENTIFIER
DF-1	ATCC	CRL-12203
HEK293-hACE2	Dr. Paul Spagnuolo, University of Guelph	NA
Specific pathogen-free eggs	Canadian Food Inspection Agency	NA
Experimental models: Organisms/strains		
Syrian hamsters	Charles River	Strain code 049
Oligonucleotides		
E_Sarbeco_F1 (′- ACAGGTACGTTAATAGTTAATAGCGT-3′)	WHO	NA
E_Sarbeco_R2 (5′-ATATTGCAGCAGTA CGCACACA-3′)	WHO	NA
probe E_Sarbeco_P1 (5′-FAM-ACACTAG CCATCCTTACTGCGCTTCG -BBQ-3′)	WHO	NA
SARS-CoV-2 Spike, forward 5′GCACCGAGTTCCCCCTCTAGATTAGAAAAAAT ACGGGTAGAACCGC CAC-3′	IDT	NA
SARS-CoV-2 Spike, reverse 5′GTTGGACCTTGG GTACGCGTTTATCAGGTGT AGTGCAGCTTCAC-3′	IDT	NA
SARS-CoV-2 Spike (SΔ19), reverse 5′GTTGGACCTTGGGTACGCGTTTATCAT CAGCA GCAAGAGCCGCAAGAACAAC-3′	IDT	NA
Software and algorithms		
PRISM	GraphPad software	Version 8
BioRad Image Lab 6.0.1. software	BioRad	Version 6.0.1
Other		
Polyvinylidene difluoride (PVDF) membrane	Cytiva	10600029

RESOURCE AVAILABILITY

Lead contact

Further information and requests for resources and reagents should be directed to and will be fulfilled by the lead contact, Dr. Sarah Wootton, University of Guelph (kwootton@uoguelph.ca).

Materials availability

Plasmids generated in this study are available upon request following execution of a material transfer agreement (MTA).

Data and code availability

- All data reported in this paper will be shared by the lead contact upon request.
- This paper does not report original code.
- Any additional information required to reanalyze the data reported in this paper is available from the lead contact upon request.

EXPERIMENTAL MODEL AND SUBJECT DETAILS

Ethics statement

The animal experiments described were carried out at the National Microbiology Laboratory (NML) of the Public Health Agency of Canada. Studies were approved by the Animal Care Committee at the Canadian Science Center for Human and Animal Health in accordance with the guidelines provided by the Canadian Council on Animal Care. All procedures including vaccinations, infections, swabs, collections were

performed under anesthesia, and all efforts were made to minimize animal suffering and to reduce the number of animals used. All SARS-CoV-2 infectious work was performed under containment level 4 (CL-4) conditions. Equal numbers of male and female hamsters four to six weeks of age were monitored daily for any adverse signs following vaccinations and infections, and were provided food and water *ad libitum*.

Cells

Vero (ATCC CCL-81) and Vero E6 (CRL-1586) cells were maintained in Minimum Essential Media (MEM) (Thermo Fisher Scientific, USA) supplemented with 10% fetal bovine serum (FBS) (Sigma-Aldrich). DF-1 cells (ATCC CRL-12203) were maintained in DMEM supplemented with 10% bovine calf serum (BCS). HEK293-hACE2 cells grown on tissue culture plates coated with L-poly-L-lysine and maintained in DMEM supplemented with 10% FBS.

METHOD DETAILS

Engineering and rescue of recombinant NDV vaccines

The full-length cDNA genome of lentogenic NDV LaSota strain was designed based on Genbank accession AF077761.1 to contain a GFP reporter gene and essential NDV-specific RNA transcriptional signals, flanked by a 5′ XbaI site and a 3′ MluI site at nucleotide position 3143 between the P and M genes. A leucine-to-alanine mutation at position 289 was also introduced into the fusion gene. The full-length recombinant clone was synthesized *de novo* using a synthesis service (GeneArt, ThermoFisher). To construct recombinant NDV expressing SARS-CoV-2 Spike, forward 5′GCACCGAGTTCCCCCTCTAGATTAGAAAAAA TACGGGTAGAACCGC CAC-3′ and reverse 5′GTTGGACCTTGGGTACGCGTTTATCAGGTGTAGTG CAGCTTCAC-3′ primers were used to amplify human codon optimized SARS-CoV-2 full-length spike. Additionally, a 19 amino acid-truncated form of the S protein (SΔ19) was amplified using the previous forward primer and a reverse 5′GTTGGACCTTGGGTACGCGTTTATCATCAGCA GCAAGAGCCGCAAGAA CAAC-3′. Infusion Cloning™ was used to insert transgenes into the NDV backbone according to the manufacturer's protocol (Takara Bio USA), with the 5′ end of the primer spanning 15 bp of homology with each end of the linearized vector including the XbaI or MluI sites. Viruses were rescued from cDNA as previously described (Santry et al., 2018), and recombinant virus identity confirmed by RT-PCR and sequencing.

Challenge virus and vaccine candidates

The SARS-CoV-2 used in this study (SARS-CoV-2; hCoV-19/Canada/ON-VIDO-01/2020, GISAID accession# EPI_ISL_425177) was isolated from a clinical specimen at Sunnybrook Research Institute (SRI)/ University of Toronto on VeroE6 cells and provided to us by the Vaccine and Infectious Disease Organization (VIDO) with permission. The virus was grown in Vero cells (ATCC, CCL-81) in minimum essential medium (Hyclone) containing 1% fetal bovine serum (FBS) and 1% L-glutamine, and a passage 2 (P2) virus stock was used for all infections. The virus was titrated on Vero cells by conventional limiting dilution assays and reported as $TCID_{50}$, as described previously (Griffin et al., 2020).

Rescued NDV-FLS, NDV-Δ19S, and NDV-GFP were grown in specific pathogen-free (SPF) eggs (Canadian Food Inspection Agency), harvested from allantoic fluid, and stocks were purified according to previously published methods (Santry et al., 2018). Recombinant NDVs were titrated in DF-1 cells by limiting dilution coupled with immunofluorescent staining (see below).

Immunofluorescence assay and titration of recombinant NDV vaccines

NDV vaccine stocks were titered on DF-1 cells (immortalized chicken embryo fibroblasts [ATCC CRL-12203]) by immunofluorescence (IFA) assay. Cells were plated in 96-well plates ($4x10^4$ cells / well) in DMEM supplemented with 2% bovine calf serum (BCS) and 5% allantoic fluid, left to adhere overnight, and infected the next day with serial 10-fold dilutions of purified allantoic fluid containing recombinant NDV vaccine. Approximately 24 hr post-infection, cells were fixed in 4% paraformaldehyde for 15 minutes at room temperature (RT), and permeabilized in 0.1% NP-40 for 10 minutes at RT. Antigens were masked in blocking buffer [5% (v/v) normal goat serum in PBS-T] either for one hour at RT or overnight at 4°C, followed by incubation with a primary mouse anti-NDV ribonucleoprotein (NBP2-11633, monoclonal; Novus Biologicals) diluted 1:2000 in blocking buffer (one hour at RT or overnight at 4°C). The secondary antibody was a goat-anti-mouse conjugated with Alexa Fluor 488 (A-11001, ThermoFisher) diluted 1:1000, which was applied in PBS-T for one hour at RT in the dark. Cells were imaged using an Axio Observer inverted

fluorescent microscope. For titration, positive wells per dilution were tallied and titer reported as $TCID_{50}$/mL, according to the Spearman-Karber method (Karber, 1931).

Vaccine characterization in DF-1 cells

DF-1 cells were seeded into 6-well plates at $1.5x10^6$ cells/well in 1 mL of DMEM with 2% bovine calf serum and supplemented with 5% allantoic fluid or 100 μg/ml of trypsin (ThermoFisher), to provide proteolytic activity. After adherence, cells were infected with either NDV-FLS, NDV-Δ19S or NDV-GFP at a multiplicity of infection (MOI) of 1 or 10 in replicate plates and incubated at 37°C. Approximately 24 hours after infection, plates were observed under an inverted phase contrast microscope to examine and document cytopathic effect. Subsequently, one set of replicate plates was used for IFA as described above, and another was used for protein extraction and western blot analysis (see below).

Sodium dodecyl-sulfate polyacrylamide gel electrophoresis (SDS-PAGE) and western blot analysis

DF-1 cells were infected in 6-well plates as described above (MOI = 1), washed with PBS and lysed for 30 min in radioimmunoprecipitation assay buffer [50 mM Tris-HCl pH 8, 150 mM NaCl, 1% NP-40, 0.5% sodium deoxycholate, 0.1% sodium dodecyl sulfate, 1X protease inhibitor cocktail (0087785, ThermoFisher)]. Cell lysates were centrifuged at 10,000 ×g for 15 min at 4°C, supernatants collected and used to quantify the protein concentration using the Pierce BCA Protein Assay Kit (ThermoFisher). For SDS-PAGE, purified virus ($1x10^7$ PFU) or virus infected cell lysates (mixed with 6x loading dye containing and 30% β-mercaptoethanol) were heated at 95°C for 10 min to denature proteins, followed by cooling on ice. The same PFU or protein amounts of each sample (ranging from 5 to 70 μg depending on the experiment) were loaded into wells of 4% stacking / 12% resolving gels, and proteins were resolved at 120 V for 1.5 h in running buffer (0.025 mM Tris-base, 0.192 M glycine, 0.1% SDS). Proteins were transferred to a 0.2 μm polyvinylidene fluoride or polyvinylidene difluoride (PVDF) membrane for 30 min, using the BioRad Trans-Blot Turbo Transfer System and associated buffer (BioRad Trans-Blot Turbo RTA Mini PVDF Transfer Kit). Following transfer, the rest of the protocol was performed as previously described (Pham et al., 2020). Briefly, the primary antibodies were incubated overnight at 4°C, and were either mouse anti-NDV ribonucleoprotein (dilution: 1:5000; NBP2-11633; Novus Biologicals), rabbit anti-SARS-CoV-2 nucleocapsid (dilution: 1:5000; PA5-81794; ThermoFisher), rabbit anti-SARS-CoV-2 S1 (dilution: 1:1000; PA5-81795; ThermoFisher) or S2 (dilution: 1:1000; NB100-56578; Novus Biologicals) subunits, or mouse anti-beta actin (diluted 1:1000; MA5-15739; ThermoFisher). The secondary antibodies were either goat anti-rabbit (G-21234) or goat anti-mouse IgG (G-21040) conjugated to horseradish peroxidase (diluted 1:2000; ThermoFisher), and incubated for 1 to 3 h at RT. Protein was detected using the Pierce SuperSignal West Pico PLUS Chemiluminescent Substrate (ThermoFisher) and the BioRad ChemiDoc MP Imaging System (BioRad Image Lab 6.0.1. software).

Neutralization of pseudotyped lentiviruses and NDV recombinant vaccines

To evaluate the contribution of the S protein to the infectivity of NDV-FLS and NDV- Δ19S, neutralization assays were conducted using immune chicken serum against NDV and murine serum raised against the S protein (see below). The chicken serum was collected from routinely vaccinated White Leghorn hens (Arkell Research Station, University of Guelph).

Briefly, mice were vaccinated intramuscularly with 10^8 infectious units (IU) of adenovirus expressing FLS, in an homologous prime-boost regimen 28 days apart. The neutralizing activity of the serum was tested on lentiviral particles pseudotyped with the truncated version of the S protein (Δ19S) and encoding the luciferase gene. Neutralization was carried out in a 96-well plate format. Approximately 10,000 HEK cells expressing the human ACE-2 receptor (HEK-ACE2) were plated in each well using L-poly-L-lysine (Millipore Sigma) to improve adherence. Equal amounts of pseudotyped lentiviruses were added to the wells (approximately $8x10^8$ relative light units [RLU] / well) and incubated with two-fold dilutions of mouse serum starting from a 1:100 dilution. Luminescence intensity was evaluated after three days using the Pierce Firefly luciferase Glow Assay Kit (ThermoFisher), and RLUs quantified using an EnSpire Multimode Plate Reader (PerkinElmer). At 1:100 dilution, the serum of vaccinated mice showed to decrease the RLU of approximately 80-90%, compared to wells incubated with the serum of non-vaccinated mice or no serum controls (Figure S2).

Neutralization of NDV-FLS and NDV- Δ19S was done in 96 well plates, separately for mouse and chicken sera. Poly-L-lysin-coated wells were seeded with HEK-ACE-2 cells and let adhere overnight. Equal amounts of NDV-FLS or NDV- Δ19S (1,000 PFU in 50 μl) were added to each well containing 1:2 dilutions of mouse or chicken serum in 50 μl, starting from an initial 1:100 dilution. Total volume for each well was 100 μl / well, and the final solution included 5% allantoic fluid. After 3 days, the magnitude of infection was evaluated by IFA for NDV ribonucleoprotein, as described above. The amount of IFA signal in the wells tested with murine serum was quantified by image analysis (ImageJ, U.S. National Institutes of Health, Bethesda, Maryland, USA), by averaging the signal intensity of the fluorescent signal using pictures from 4 different wells.

Determination of mean death time (MDT)

The MDT was determined for the two vaccine candidates and the control (NDV-FLS, NDV-SΔ19, and NDV-GFP). The virus stocks were equalized to a starting titer of 6.14×10^6 $TCID_{50}$/mL, and each virus stock was serially diluted from 10^{-1} to 10^{-8} in PBS. Dilutions from 10^{-4} to 10^{-8} were inoculated into specific pathogen-free eggs (Canadian Food Inspection Agency) at 9 to 11 days of embryonation. For each virus, five eggs were inoculated per dilution (100 μL / egg). The experiment was run in duplicate 3 to 4 hours apart, resulting in 50 eggs used for each virus. After virus inoculation, the eggs were incubated for up to 7 days and checked twice daily for embryo mortality; after the first 24 hr after inoculation, allantoic fluid was collected from all dead embryos to check for presence of NDV by hemagglutination assay (HA), according to standards methods (McGinnes et al., 2006). The MDT was recorded as the time (in hours) taken by the minimal lethal dose (highest dilution) to kill all five eggs in the dilution series. If no minimal lethal dose was observed by the end of the experiment (seven days post-inoculation), it was concluded that the MDT was > 168 hrs, and HA was performed on the allantoic fluid collected from eggs inoculated with the lowest virus dilution (10^{-4}) to confirm NDV infection.

Lyophilization of NDV-FLS

Triplicate samples of freshly harvested allantoic fluid containing NDV-FLS were aliquoted into 15mL conical tubes in 1mL volumes. Aliquots were either left untreated or adjusted to a final concentration of 5% sucrose, 5% sucrose/5% Iodixanol or mixed 1:1 with a solution containing 10% lactose, 2% peptone, 10mM Tris-HCl, pH 7.6. Using an LABCONCO Freeze Dry system Freezone®4.5, samples were immediately lyophilized at 44 x 10-3 MBAR and -52°C for 16 hours. Lyophilized samples were stored at 4°C for 48 hours before being resuspended in 1 mL of 5% sucrose/PBS and titered. Three 1 mL aliquots of allantoic fluid containing NDV-FLS were adjusted to 5% sucrose and frozen at -70°C before titering. An additional three 1 mL aliquots were used to titer NDV-FLS in allantoic fluid immediately following harvest from eggs. All samples were titered by $TCID_{50}$ on DF-1 cells as described above.

To determine presence of S protein in the reconstituted preparations, lyophilized (10% lactose and 2% peptone group, only) and reconstituted NDV-FLS was compared to NDV-FLS stored at -70°C (purified preparation frozen at -70°C in sucrose). Equal amounts of virus preparations (10^7 PFU, as determined by post-reconstitution titers) were loaded on SDS-PAGE gel, transferred to a nitrocellulose membrane and immunoblotted for the S protein using a rabbit anti-SARS-CoV-2 S2 subunit (dilution: 1:1000; NB100-56578; Novus Biologicals), as described in the previous section. To determine the ability of lyophilized and reconstituted virus to express S protein in infected cells, DF-1 cells were infected with the same amounts of reconstituted or frozen virus (MOI = 0.5). Whole cell lysates were harvested 24 hrs post-infection, immunoblotting for the S protein was conducted as above.

Immunization and infection of Syrian hamsters

For initial immunization and booster immunization of hamsters, groups of ten Syrian Golden hamsters (five male and five female, four to six weeks of age; Charles River) were anaesthetized with inhalation isoflurane and administered 1×10^7 PFU of recombinant NDV-GFP, NDV-FLS, or NDV-Δ19S via the intranasal (IN) route. For IN vaccinations, anaesthetized hamsters were scruffed and vaccines were delivered in a 100 μL volume (q.s. with PBS) through the nares (50 μL per nare). Animals had their mouths held closed to ensure inhalation through the nose. After recovery from anesthesia hamsters were monitored daily for any adverse signs following vaccine administration.

For SARS-CoV-2 infection following immunization, hamsters were moved into a CL-4 facility and then anaesthetized with inhaled isoflurane. Hamsters were then infected with 10^5 $TCID_{50}$ of SARS-CoV-2 via

the same IN method described above. After recovery from anesthetic hamsters were monitored daily throughout the course of infection. Body weights and temperatures of hamsters were recorded daily.

Microscopic pathology

At day five post-challenge, six hamsters per group were euthanized, and the proximal and distal lobes of the lung from each hamster were sampled and fixed in 10% buffered formalin, followed by routine paraffin embedding, sectioning, and staining with hematoxylin and eosin (HE). The magnitude of microscopic lesions caused by SARS-CoV-2 in the lungs of vaccinated and control mice was evaluated histologically using two semi-quantitative scoring systems based on the presence of nominal categories (Tables S1 and S2) (Meyerholz and Beck, 2020) and extent of the pulmonary parenchyma affected (Table S3) (Imai et al., 2020). Assessment was carried out taking into consideration all the sections available for evaluation. Slides were scored by a board-certified veterinary anatomic pathologist (LS), who was blind to the treatment of the experimental groups (group de-identification).

Detection of SARS-CoV-2 RNA in tissues and swabs of infected hamsters

Oropharyngeal and rectal swabs were obtained and stored in MEM + 2% penicillin-streptomycin. For viral RNA detection, 140μL of the medium containing the swab was used for viral lysis and extraction using the QIAamp Viral RNA mini kit. For viral RNA detection, tissue samples were thawed, weighed, and then homogenized in 600 μL RLT buffer (Qiagen) using a Bead Ruptor Elite Bead Mill Homogenizer (Omni International) with a stainless steel bead for at 4 m/s for 60 seconds. Viral RNA from 30 mg samples of each tissue was extracted with the RNeasy Plus Mini kit (Qiagen) according to manufacturer's instructions, and viral RNA from swab samples was extracted with the QIAamp Viral RNA Mini kit (Qiagen) also according to manufacturer's instructions. Detection of SARS-CoV-2 E gene was performed using TaqPath 1-Step Multiplex Master Mix kit (Applied Biosystems) and was carried out on a QuantStudio 5 real-time PCR system (Appiled Biosystems), as per the manufacturer's instructions. RNA was reverse transcribed and amplified using the primers reported by the WHO and include E_Sarbeco_F1 (5′- ACAGGTACGTTAATAGTTAATAGCGT-3′) and E_Sarbeco_R2 (5′-ATATTGCAGCAGTA CGCACACA-3′) and probe E_Sarbeco_P1 (5′-FAM-ACACTA GCCATCCTTACTGCGCTTCG -BBQ-3′). A standard curve produced with synthesized target DNA was run with every plate and used for the interpolation of viral genome copy numbers.

Detection of infectious SARS-CoV-2 in tissues and swabs of infected hamsters

For infectious virus assays, thawed tissue samples were weighed and placed in 1 mL of minimum essential medium supplemented with 1% heat-inactivated fetal bovine serum (FBS) and 1x L-glutamine, then homogenized in a Bead Ruptor Elite Bead Mill Homogenizer (Omni International) at 4 m/s for 30 seconds then clarified by centrifugation at 1,500 xg for 10 minutes. Prior to titration procedures, oropharyngeal and rectal swabs stored in MEM + 2% penicillin-streptomycin were vortexed and centrifuged briefly. Samples were serially diluted 10-fold in media and dilutions were then added to 96-well plates of 95% confluent Vero cells containing 50 μL of the same medium in replicates of three and incubated for five days at 37°C with 5% CO_2. Plates were scored for the presence of cytopathic effect on day five after infection. Titers were calculated using the Reed-Muench method, and reported as $TCID_{50}$ units.

Determination of antibody responses by ELISA and PRNT assay

For detection of anti-SARS-CoV-2-specific antibody responses, all hamsters were bled via jugular vein bleeds for serum on days 21, 29, 49, and 56 post-first vaccination. For ELISAs for detection of total IgG detection, SARS-CoV-2 spike- and nucleoprotein-specific responses were assessed using an in-house assay. A 1:400 dilution of serum was carried out in duplicate and added to plates pre-coated with both spike and nucleoprotein in the same assay wells. IgG was detected with a peroxidase-labeled polyclonal goat anti-hamster IgG (H+L) (KPL).

For virus PRNT (plaque reduction neutralization assays), serum samples were heat-inactivated at 56°C for 30 minutes and diluted two-fold from 1:40 to 1:1280 in DMEM supplemented with 2% FBS. Diluted sera were incubated with 50 PFU of SARS-CoV-2 at 37°C and 5% CO2 for 1 hour. The sera-virus mixtures were added to 24-well plates containing Vero E6 cells at 100% confluence, followed by incubation at 37°C and 5% CO2 for 1 hour. After adsorption, 1.5% carboxymethylcellulose diluted in MEM supplemented with 4% FBS, L-glutamine, non-essential amino acids, and sodium bicarbonate was added to each well and plates were incubated at 37°C and 5% CO2 for 72 hours. The liquid overlay was removed and cells were

fixed with 10% neutral-buffered formalin for 1 hour at room temperature. The monolayers were stained with 0.5% crystal violet for 10 minutes and washed with 20% ethanol. Plaques were enumerated and compared to a 90% neutralization control. The PRNT-90 endpoint titer was defined as the highest serum dilution resulting in a 90% reduction in the number of plaques. PRNT-90 titers $\geq$1:40 were considered positive for neutralizing antibodies.

Hematological and biochemical analysis of blood and serum

Complete blood counts were carried out using a VetScan HM5 hematology system (Abaxis Veterinary Diagnostics), as per the manufacturer's instructions. Analysis of serum biochemistry was performed with a VetScan VS2 analyzer (Abaxis Veterinary Diagnostics), as per the manufacturer's instructions.

Cytokine mRNA analysis

RNA was extracted from proximal lung samples as described above using a RNeasy Plus Mini Kit (Qiagen), which includes a genomic DNA elimination step, as per the manufacturer's instructions. Expression of IFNγ, IL-2, IL-4, IL-10, IL-1b, FoxP3, TGF-β, VEGF, IL-6, and TNFα mRNA was analyzed using the one-step TaqPath Master Mix kit using the primer/probe sets described previously (Warner et al., 2017). Ribosomal protein L18 (RPL18) was used as an internal control. All RT-qPCR assays were performed on a QuantStudio 5 instrument (Applied Biosystems). Expression is reported as Log_2 of the fold-change for each gene as calculated using the ΔΔCt method compared with expression of the same genes in sex-matched control tissues that were unvaccinated and uninfected.

QUANTIFICATION AND STATISTICAL ANALYSIS

Mean scores between experimental groups were compared using analysis of variance (ANOVA) with Tukey's post-hoc (lyophilization experiment) or Holm Sidak (neutralization) tests for multiple comparisons, two-way ANOVA (serology), non-parametric Mann-Whitney or Kruskal-Wallis test followed by the Dunn's method for multiple comparisons (all other tests and pathology data), with significance set at $p < 0.05$ as implemented in GraphPad software version 8.0.0 (San Diego, California, USA, www.graphpad.com). Data are represented as scatterplots with median, median with range, or average with standard deviation (see figure legends).